AD NUMBER

**AD431840**

LIMITATION CHANGES

TO:

**Approved for public release; distribution is unlimited. Document partially illegible.**

FROM:

**Distribution authorized to U.S. Gov't. agencies and their contractors;
Administrative/Operational Use; 18 FEB 1964.
Other requests shall be referred to Office of Naval Research, Arlington, VA 22203. Document partially illegible.**

AUTHORITY

**ONR ltr dtd 4 May 1977**

# Measurement of Fluid Properties for Magnetoplasmadynamic Power Generators

## Third Quarterly Technical Summary Report

## (1 November 1963—31 January 1964)

Contract No. Nonr-4104(00)

Order No.: ARPA 420 Project Code No. 3980

Engineering Department Report No. 3743



Allison Division

General Motors Corporation

Indianapolis, Indiana

(5) 37800

(6) **Measurement of Fluid Properties for Magnetoplasmadynamic Power Generators**

**Third Quarterly Technical Summary Report**

**(1 November 1963—31 January 1964)**

**Contract No. Nonr-4104(00)**

**Order No.: ARPA 420** **Project Code No. 3980**

**Engineering Department Report No. 3743**

**18 February 1964**

(9) Quarterly Technical summary rep't. no 3, 1 Nov 63 - 31 Jan 64

(10)

By R. T. Schneider,
H. E. Wilhelm
W. Woerner and
R. O. Whitaker.

Approved: F. G. Myers

Dr. F. G. Myers
Director of Research

(8)

## FOREWORD

This technical summary report was prepared by the Research Department of the Allison Division of General Motors Corporation. The work reported was accomplished under Contract Nonr-4104(00).

The program was sponsored by the Advanced Research and Project Agency through the Power Branch of the Office of Naval Research under the direction of Dr. J. Huth of ARPA and Mr. J. A. Satkowski of ONR.

TABLE OF CONTENTS

## LIST OF ILLUSTRATIONS

# I. INTRODUCTION

This third Quarterly Technical Summary Report describes the progress made in the period 1 November through 31 January. During this period the MPD section was incorporated into the closed loop device. A large number of runs with pure helium were made. Also, four runs were made with helium seeded with cesium.

This report describes the final assembly of the MPD test section, the design and construction of the fast readout unit for the 48-pin electrodes, and the results of the runs with pure helium.

Experience gained from the runs with helium seeded with cesium is discussed.

## II. RESUME OF PROGRESS

### MANUFACTURE OF CLOSED LOOP DEVICE

During this report period the diagnostic closed loop MPD device was completed.

The following changes were made in the system.

- The charcoal filters were removed. Only the absolute filters remain in the system.
- A calibration unit for the heat balance flow meter was designed, installed, and checked out.

### FIRST TEST RUNS

A large number of runs with pure helium were made during which pressure probe and thermocouple measurements were obtained. It was possible to establish calibration curves for all parameters to set the system for a certain mass flow at a given temperature. The impurities were checked spectroscopically. For water vapor and $O_2$, continuous sampling techniques were employed.

To date four runs with helium seeded with cesium have been made. A typical but preliminary value for a gas temperature of 1000°K was 1.0 volt generated voltage and 0.4 ma generated current.

The system remained operable. More runs with helium seeded with cesium are scheduled. It is anticipated that after completion of these runs a few changes in the system design will be made.

### THEORETICAL INVESTIGATIONS

#### Equilibrium

A new equation was derived describing on a statistical basis the ionization equilibrium of plasmas in magnetic fields.

Nonequilibrium

Field equations and transport relations for a reacting multitemperature plasma are presented in this report. The theory involved is based on the classical approximation neglecting the perturbation of the particle distribution function by the reactions.

## III. THE ALLISON DIAGNOSTIC CLOSED LOOP MPD DEVICE

### FINAL ASSEMBLY OF THE MPD TEST SECTION

Figure 1 is the schematic diagram of the MPD test section. Figure 2 is a photographic view of the section. The test section has been designed specifically for diagnostic investigation of plasma properties. Emphasis has been placed on versatility, ease of maintenance, and simplicity.

As shown in Figure 1, the test section consists of a flow channel electrode block, observation ports, and electromagnetic assembly. Figure 3 shows the tantalum flow channel with observation window. The plasma enter from the right. The vertical, rectangular pieces are the electrode ducts. The horizontal, cylindrical pieces are radiation shields which cover the tantalum channel.

The tantalum channel and the electrode ducts are lined with high purity alumina panels to provide electrical insulation with respect to currents induced in the $\vec{v} \times \vec{B}$ interaction. They serve also as protection for the tantalum walls. The linings, shown in Figure 4, are easy to replace. Figure 4 is a view into one of the electrode ducts. One observation window can be seen from inside the duct. The rectangular opening which is also visible inside is the exit of the plasma channel.

The tantalum duct is housed in a stainless steel structure containing a helium protective atmosphere to prevent oxidation. Figure 5 is a close view of the MPD Section. Figure 6 is an assembly view of entire section. The electrodes consist of 48 platinum pins shrunk into an alumina block. One of the electrodes is shown in Figure 7. The two pins at the left in Figure 7 serve as supports for a Pt-PtRh thermocouple. An electrical lead from the pin is connected to a corresponding pin of a 50-pin hermetically sealed connector. The connector is visible in Figure 6.

### DIRECT READOUT UNIT

A direct readout unit was developed to display the generated voltages of each pin separately on an oscilloscope screen. The voltages developed between each pin in the upper electrode and its corresponding pin in the lower electrode are indicated by the oscilloscopic display depicted in Figure 8.

Relatively high voltages are indicated for the pin pairs of the No. 5 column. Low voltages are indicated for the right half of the first pin-pair row. The system, as presently constructed, permits scanning of all voltages in approximately one second. The scanning may be stopped and the voltages appearing across the pin-pairs of any one column may be continually displayed. The circuitry is shown in Figure 9. The console is shown in Figure 10. The heart of the scanning unit is a solenoid-driven, 24-position, ten-pole stepping switch. Alternate positions are grounded--leaving twelve active positions.

Consider row No. 1 of the top electrode. The twelve pins are connected by cable to the twelve active positions of the row No. 1 Switch—Top. The twelve pins of row No. 1 of the bottom electrode similarly connect to the active positions of row No. 1 Switch—Bottom. Operation of the switch causes successive pin pairs to be connected to the differential amplifier. The differential amplifier feeds to the first trace of the oscilloscope. A Tektronix oscilloscope fitted with a four-input plug-in unit is employed. The remaining rows of electrode pins provide similar inputs to the oscilloscope.

It is desirable to place variable loads across the pin pairs. These are provided by the 1000-ohm load rheostats as indicated in Figure 9. Knobs for adjusting appear in Figure 10.

It is also desirable to be able to connect the pins in various series and parallel combinations. To facilitate this, the ends of each rheostat are brought to banana plugs on the front panel. These plugs are located in pairs just beneath each rheostat adjusting knob as indicated in Figure 10.

At present, the stepping switch moves at only one speed—maximum. The jar associated with operation of the solenoid causes contact bounce which shows up as noise on the oscilloscope traces. It is planned to provide variable rates of scan. Slower rates of scan will permit the contact bounce to die out before the next step is taken.

At present, scanning is initiated by depression of the scanning switch shown in Figure 10. This switch applies power to the solenoid and also delivers a trigger signal to the scope for initiating scanning in the scope. This system operates very well for a single rate of scan. Introduction of variable rates of scan makes a change desirable. It is planned to remove the scope triggering signal and in its place feed the scope horizontal sweep from voltages derived from the stepping switch. This will ensure that each voltage appears in proper position regardless of rate of scan.

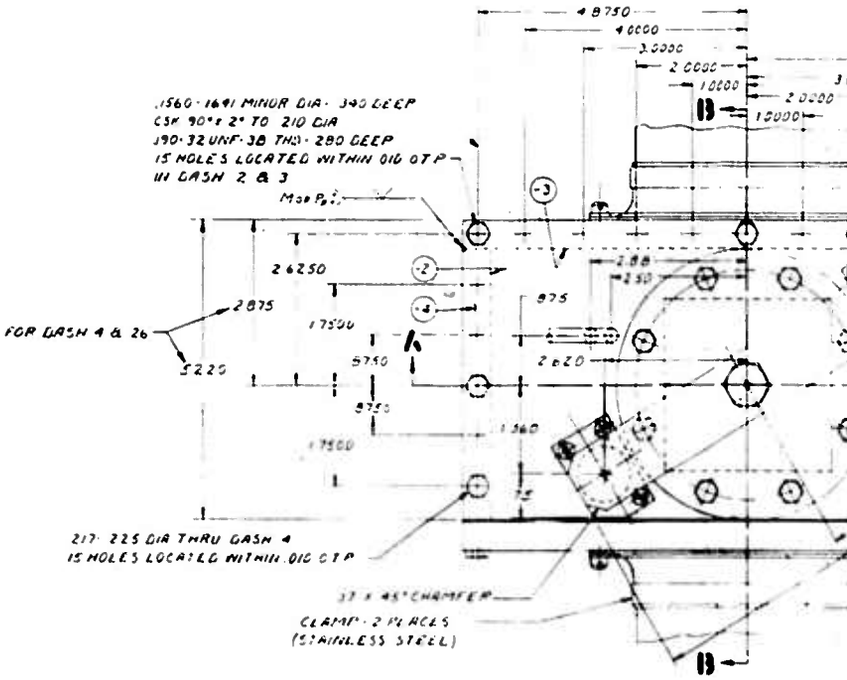
.1560-.1641 MINOR DIA-.340 DEEP
CSK 90°±2° TO .210 DIA
.190-.32 UNF-3B THD-.280 DEEP
15 HOLES LOCATED WITHIN .010 O T P
IN DASH 2 & 3
FOR DASH 4 & 26
.2217-.225 DIA THRU DASH 4
15 HOLES LOCATED WITHIN .010 O T P
.32 x 45° CHAMFER
CLAMP-2 PLACES
(STAINLESS STEEL)

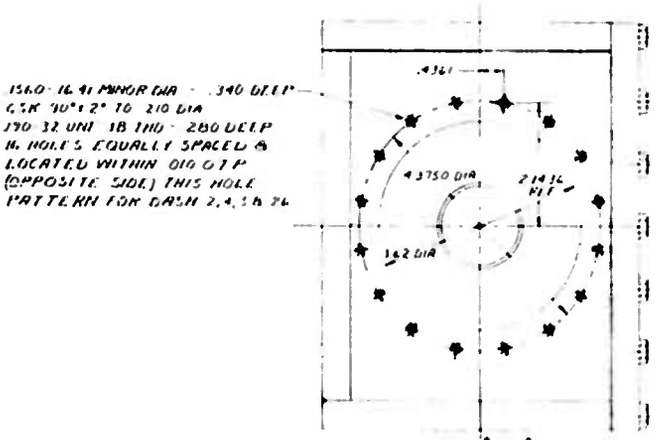
.1560-.1641 MINOR DIA-.340 DEEP
CSK 90°±2° TO .210 DIA
.190-.32 UNF-3B THD-.280 DEEP
16 HOLES EQUALLY SPACED &
LOCATED WITHIN .010 O T P
(OPPOSITE SIDE) THIS HOLE
PATTERN FOR DASH 2,4,5 & 26
VIEW A A
DASH 27, 30 & 31 OMITTED

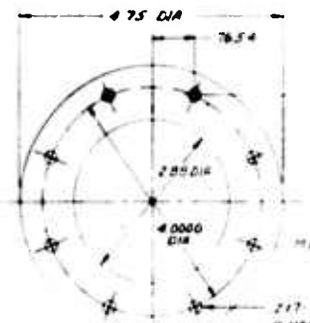
VIEW D D

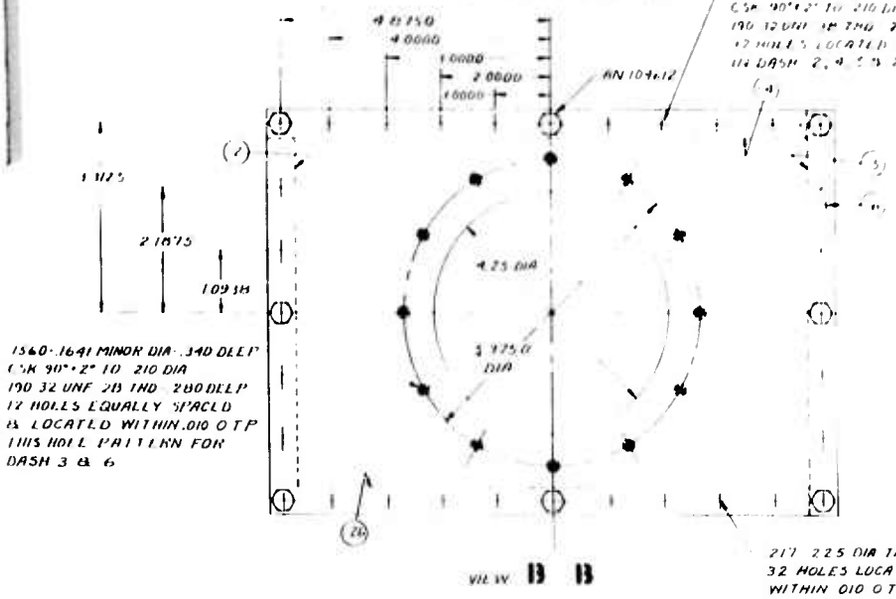
.1560-.1641 MINOR DIA-.340 DEEP
CSK 90°±2° TO .210 DIA
.190-32 UNF-3B THD-.280 DEEP
12 HOLES EQUALLY SPACED
& LOCATED WITHIN .010 O T P
THIS HOLE PATTERN FOR
DASH 3 & 6
.2217-.225 DIA THRU DASH 6
32 HOLES LOCATED
WITHIN .010 O T P
VIEW B B

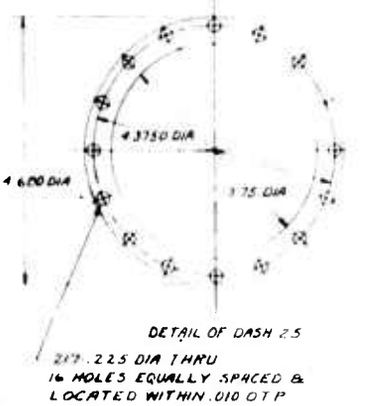
DETAIL OF DASH 25
.2217-.225 DIA THRU
16 HOLES EQUALLY SPACED &
LOCATED WITHIN .010 O T P

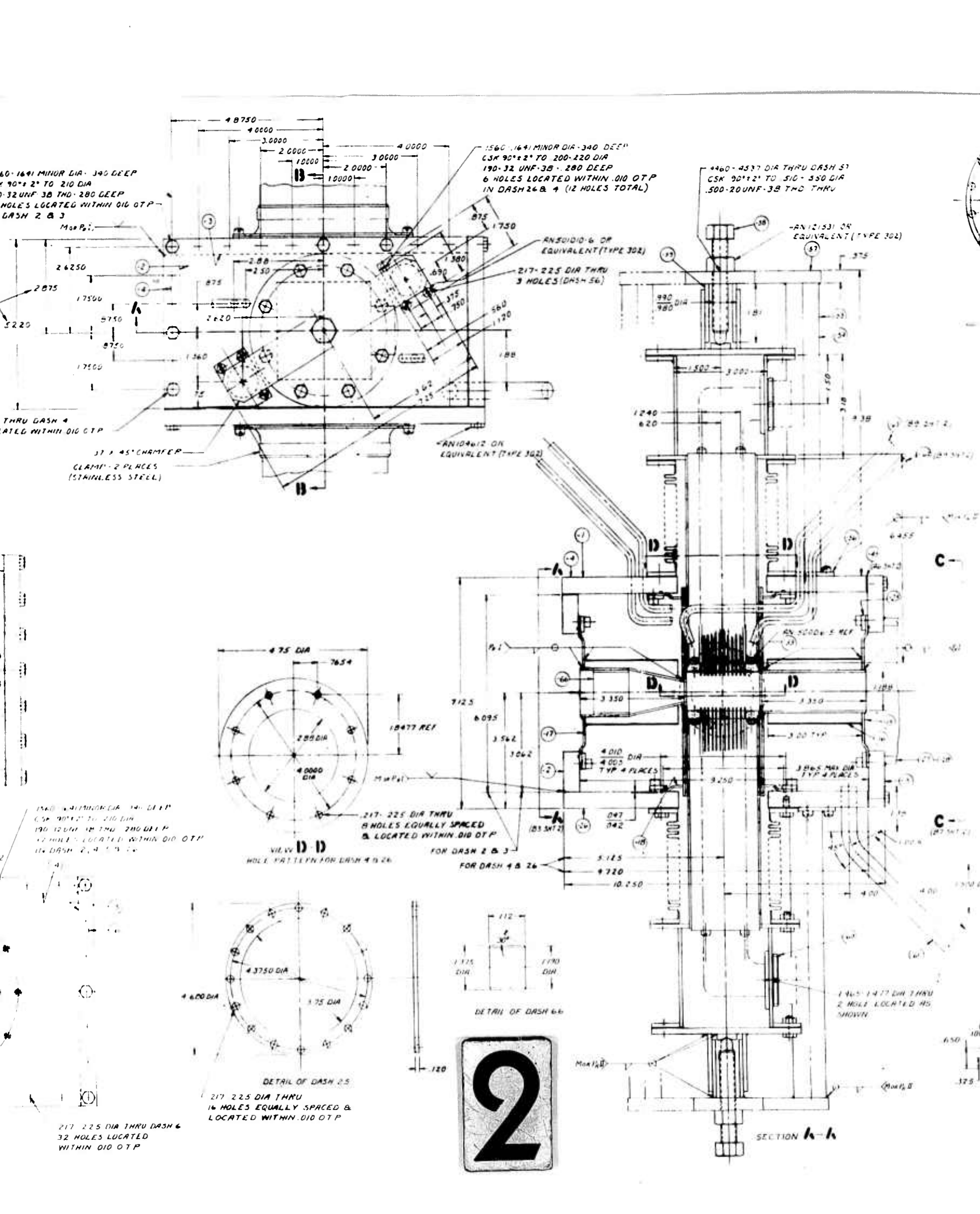
.1560-.1641 MINOR DIA-.340 DEEP
CSK 90°±2° TO .200-.220 DIA
.190-.32 UNF-3B-.280 DEEP
6 HOLES LOCATED WITHIN .010 DTP
IN DASH 2 & 4 (12 HOLES TOTAL)
.4460-.4537 DIA THRU DASH 53
CSK 90°±2° TO .510-.550 DIA
.500-.20 UNF-3B THD THRU
-AN5010-6 OR EQUIVALENT (TYPE 302)
-AN12153 OR EQUIVALENT (TYPE 302)
.217-.225 DIA THRU 3 HOLES (DASH 56)
-AN4012 OR EQUIVALENT (TYPE 302)
45° CHAMFER
CLAMP-2 PLACES (STAINLESS STEEL)
.217-.225 DIA THRU
8 HOLES EQUALLY SPACED
& LOCATED WITHIN .010 DTP
FOR DASH 2 & 3
FOR DASH 4 & 24
VIEW D-D
HOLE PATTERN FOR DASH 4 & 24
DETAIL OF DASH 25
DETAIL OF DASH 66
.217-.225 DIA THRU DASH 6
32 HOLES LOCATED
WITHIN .010 DTP
.217-.225 DIA THRU
16 HOLES EQUALLY SPACED &
LOCATED WITHIN .010 DTP
.1465-.1477 DIA THRU
2 HOLES LOCATED AS
SHOWN
SECTION A-A
2

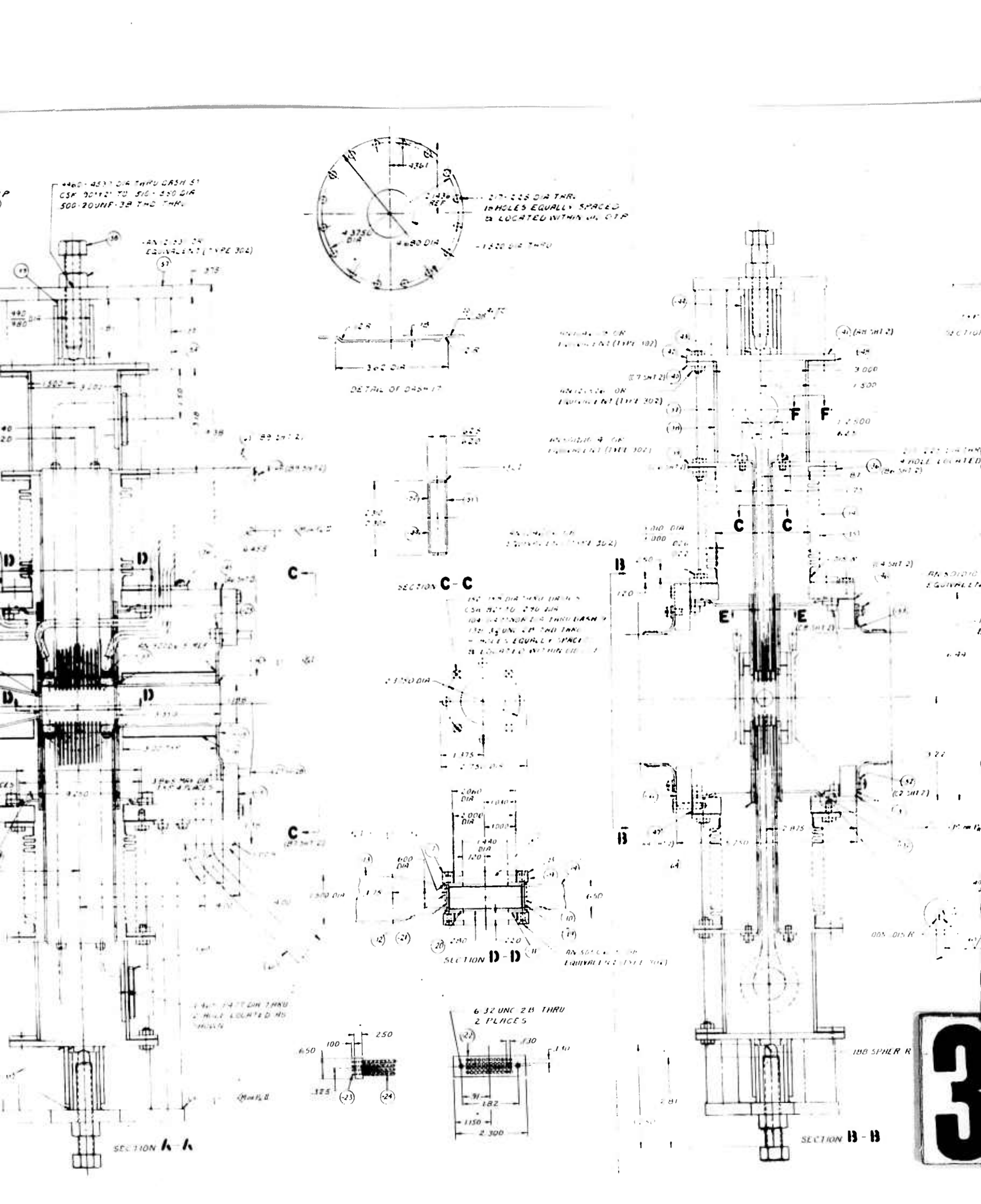
SECTION A-A
SECTION B-B
SECTION C-C
SECTION D-D
DETAIL OF DASH 17
6 32 UNC 2B THRU
2 PLACES
3

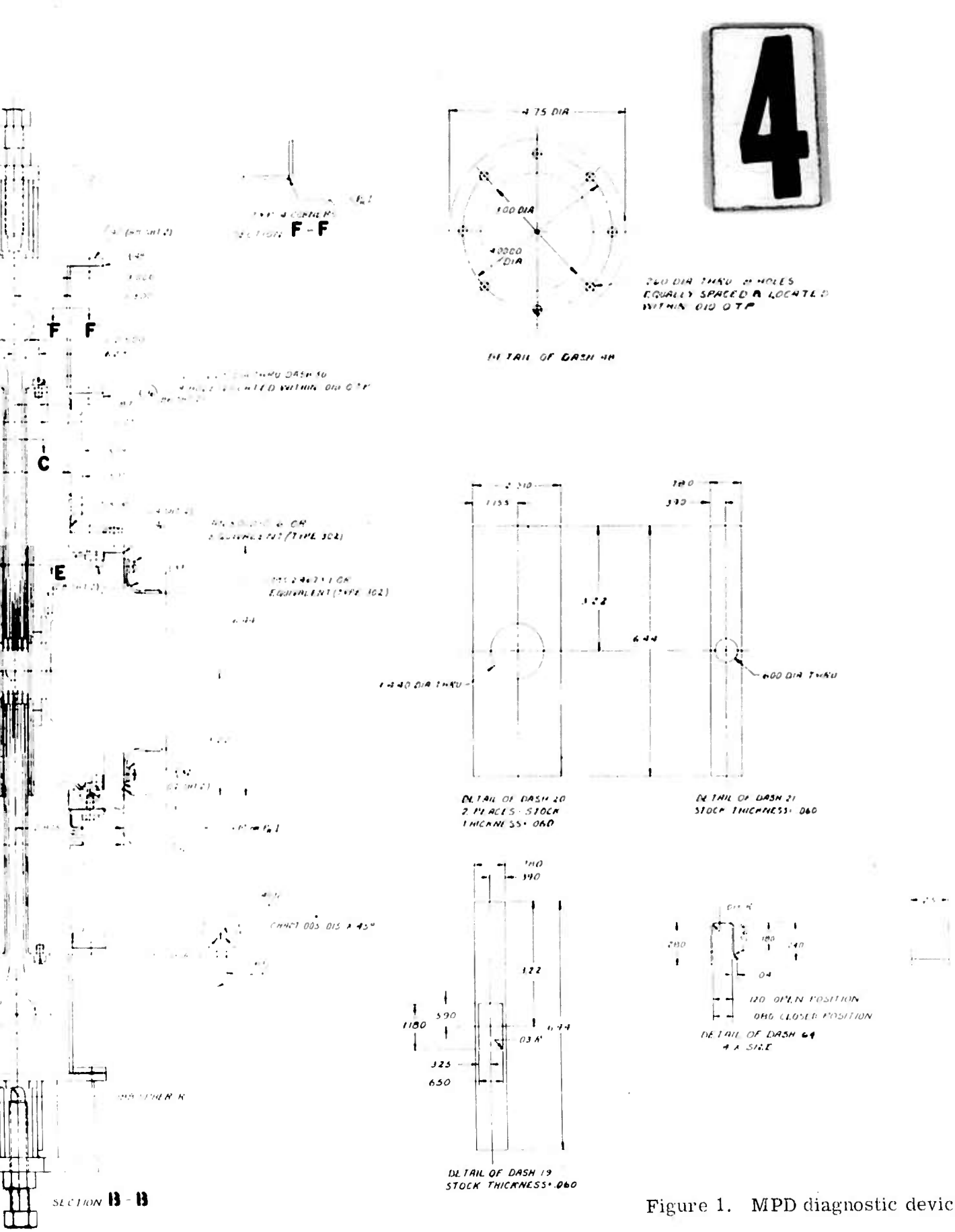


Figure 1. MPD diagnostic device.

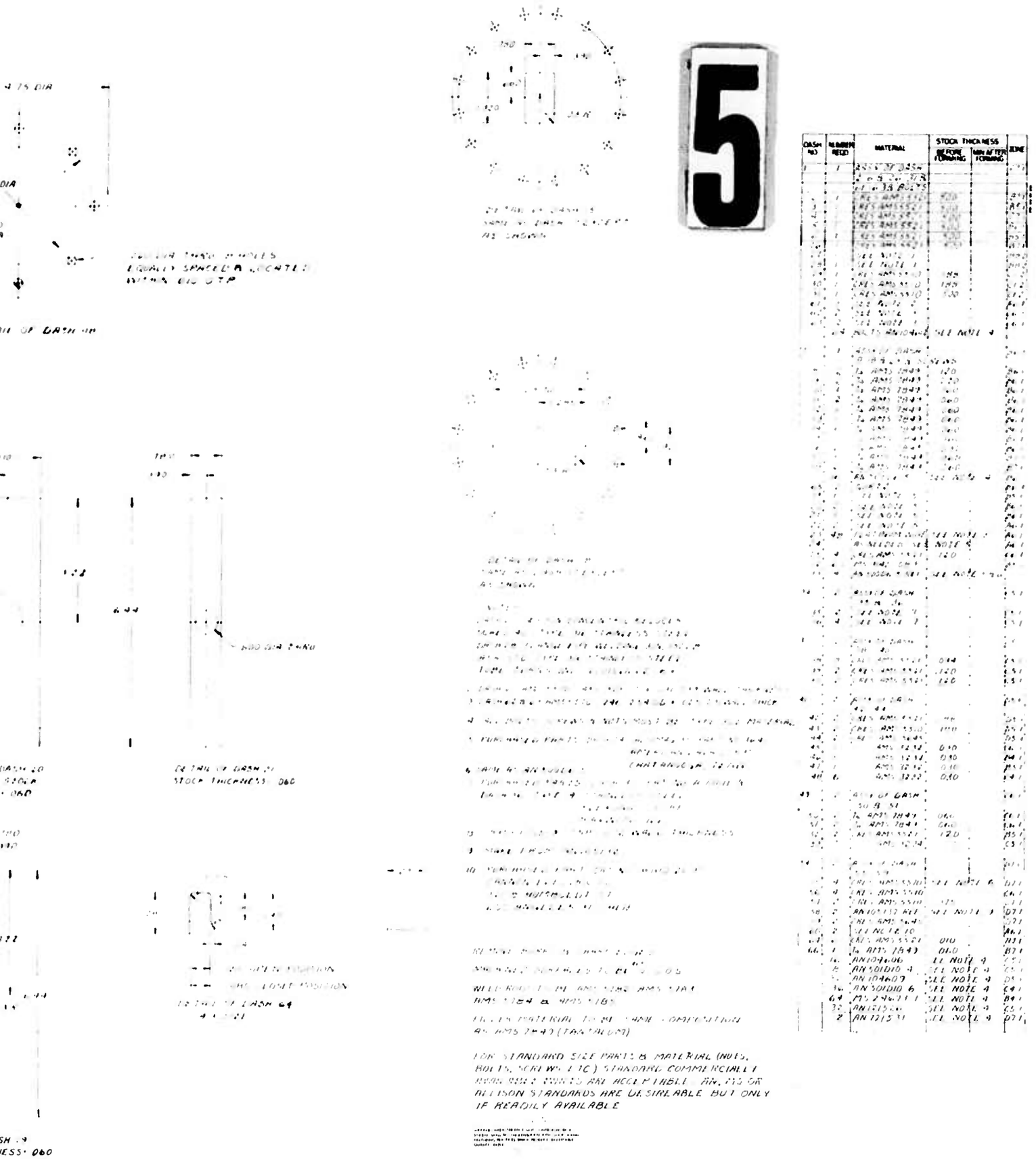


Figure 1. MPD diagnostic device.

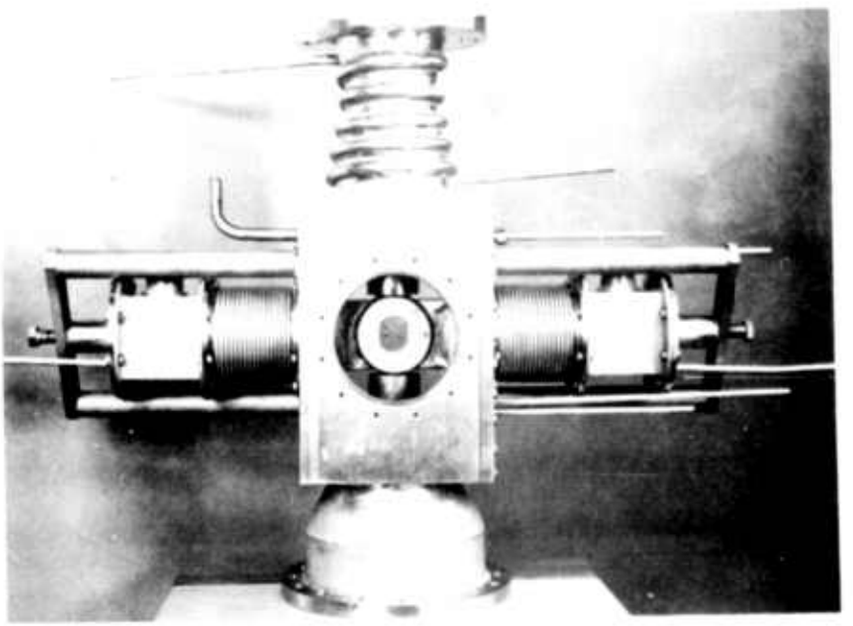

Figure 2. MPD test section.

Figure 3. Tantalum flow channel with observation window.

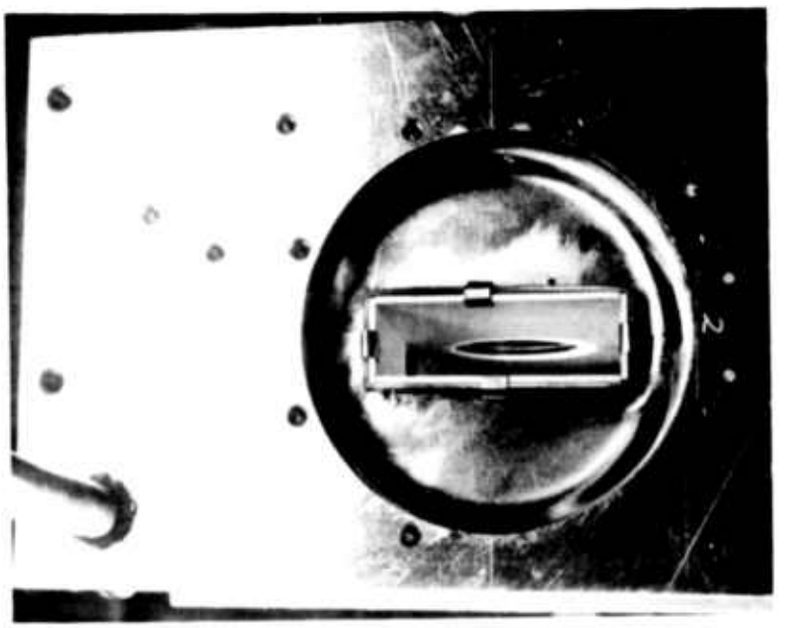

Figure 4. Electrode duct showing ceramic lining.

Figure 5.
Closeup view of MPD section.

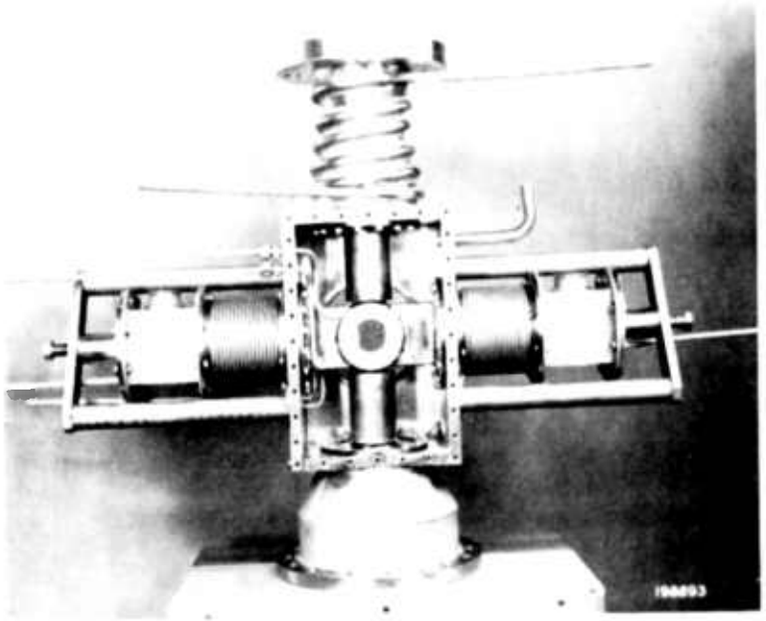

Figure 6. Assembly view of MPD section.

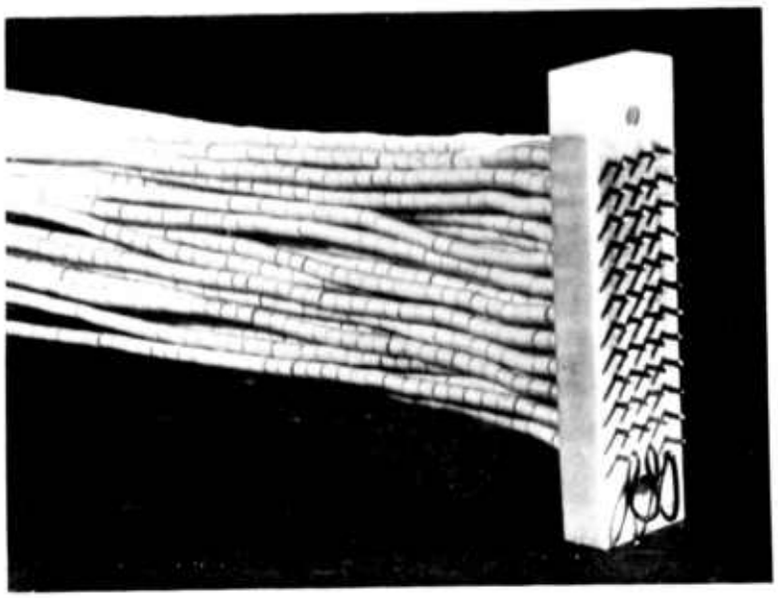

Figure 7. Electrode consisting of 48 platinum pins.

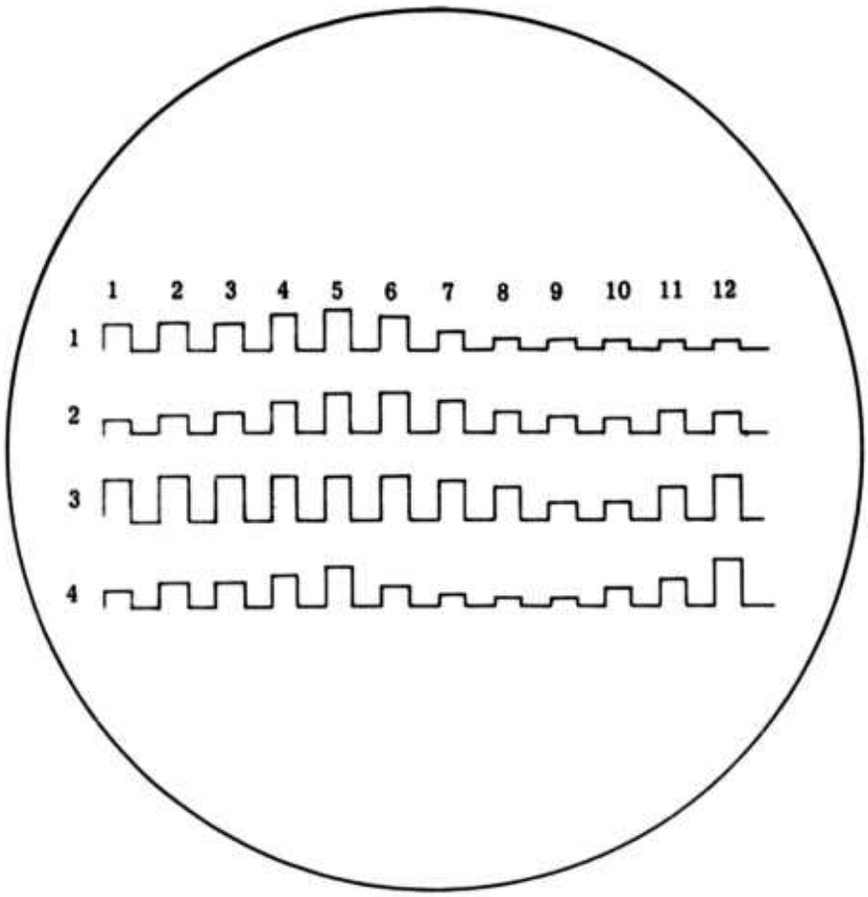


Figure 8. Oscilloscopic display of pin-pair voltages.

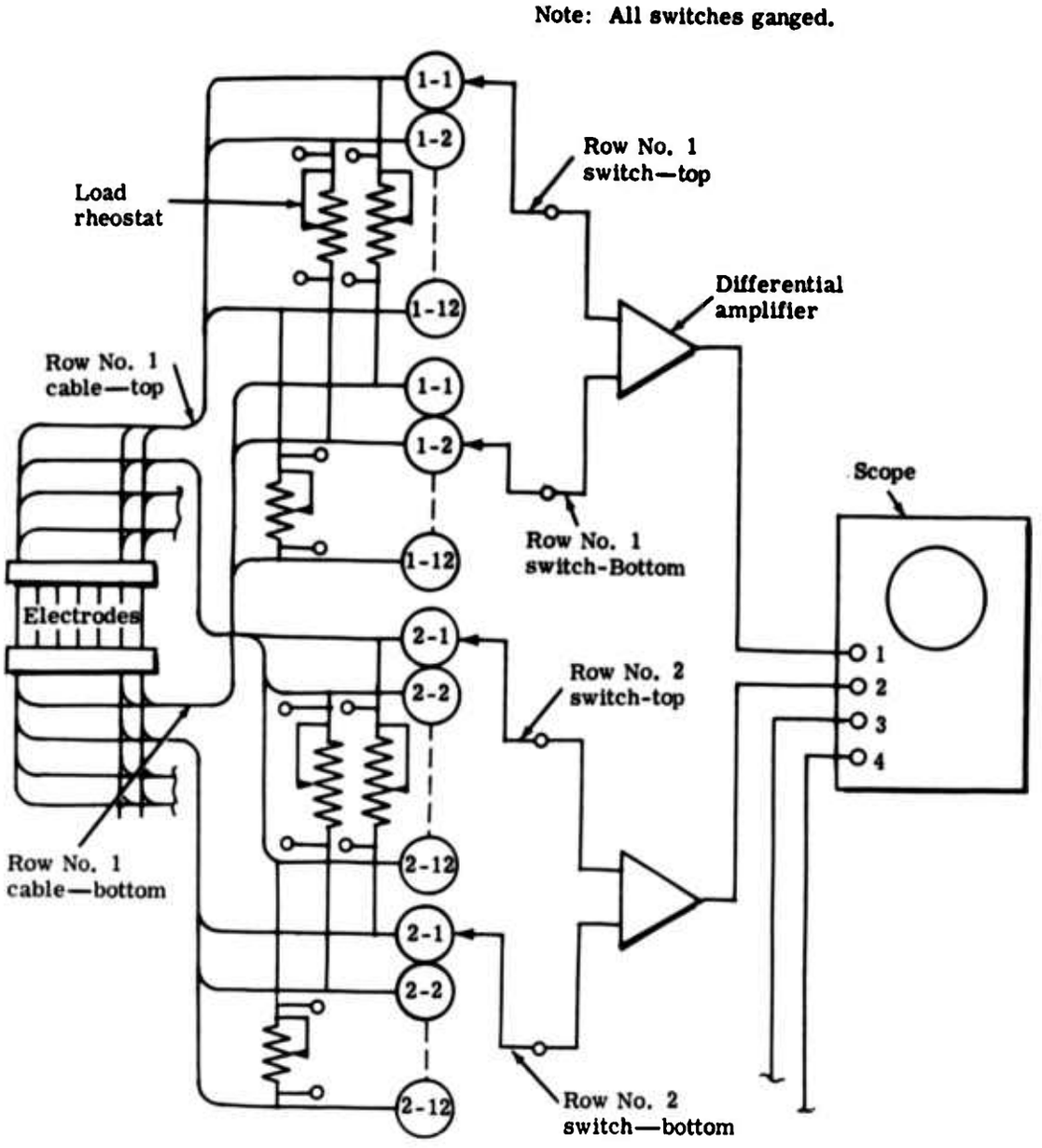


Figure 9. Circuitry schematic.

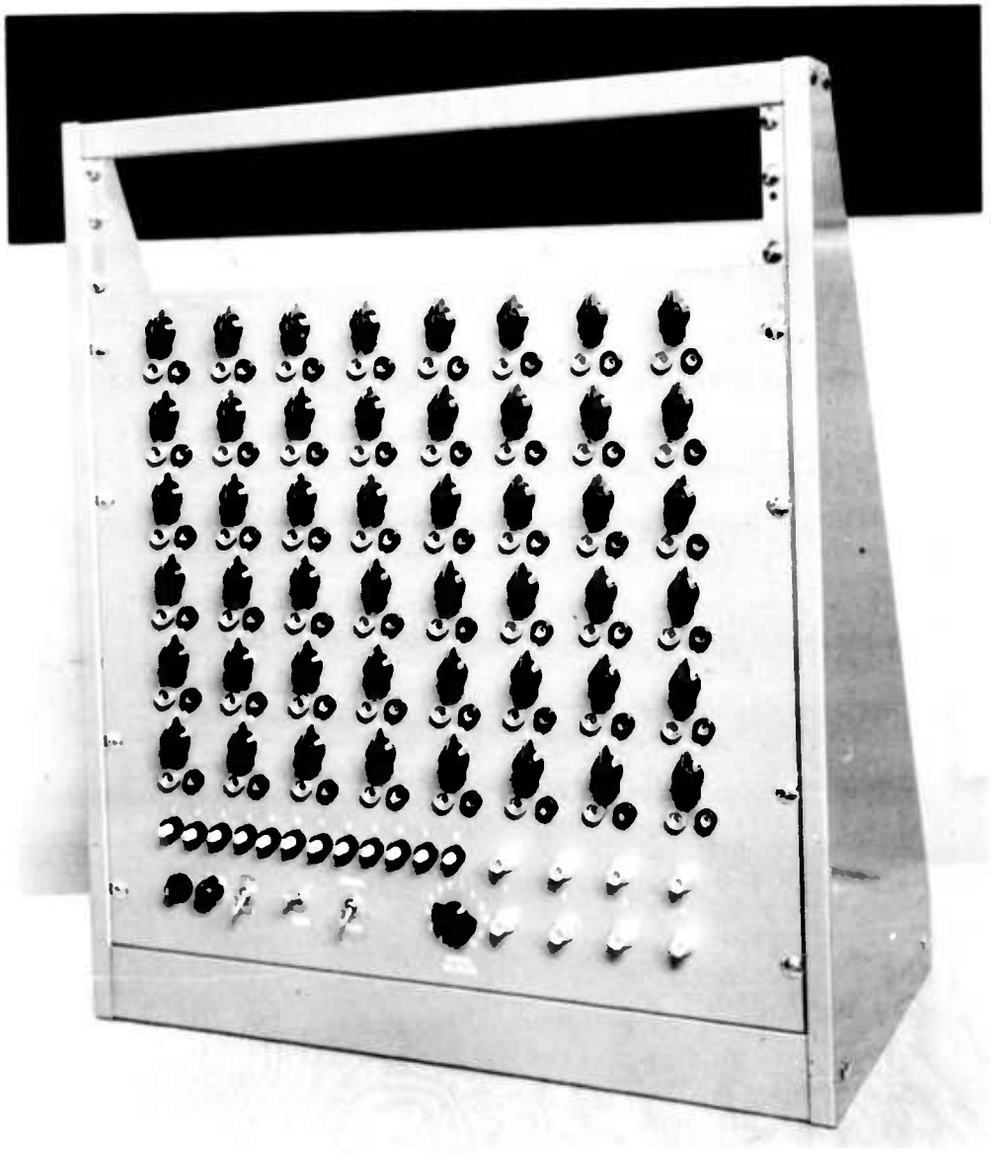

Figure 10. Direct readout unit.

## IV. TEST RESULTS

### RUNS WITH PURE HELIUM

The runs with pure helium served as a shakedown for the overall performance of the system.

The main point of interest was to establish calibration curves for different mass flows to be able to produce a given temperature by varying the heater power input.

Other points of interest were the performance of the heater, the filters, the helium compressor, and the cooling system.

A large number of runs were made and about 25 hours of running time were accumulated. Between the runs the system was dismantled for inspection. The highest temperature was 1500°K. The highest mass flow was 8.74 gm/sec.

The runs with pure helium caused no attack on the tantalum parts of the test section. Also, the ceramic parts showed no attack. However, a slight deposit on the ceramic parts was found. Spectroscopic analysis made of the deposit indicated W, Ta, Th, and traces of Sn and Be. All these materials are present in the heater, the main source of impurities. Judging from the amount of deposit and the running time involved, one can estimate that these impurities do not amount to more than 1 ppm. It was not possible to detect these impurities with spectroscopic analysis of the gas during the runs.

Measurements of water vapor content and oxygen content were continuously monitored. The water vapor was kept down to 10 ppm; the oxygen content varied from 0.5 to 1.5 ppm.

Static and total pressure probes were installed to obtain calibration curves for heater power input settings. The results of these probe measurements are shown in Figures 11 and 12. Figure 11 is a plot of gas temperature versus heater power input, while Figure 12 gives the gas velocity versus heater power input. Both gas properties are from the center of the test section. Figure 13 gives a plot Mach number versus power input, which was derived from Figures 11 and 12. It is intended to repeat these runs with thermocouples in place of the probes and compare the results.

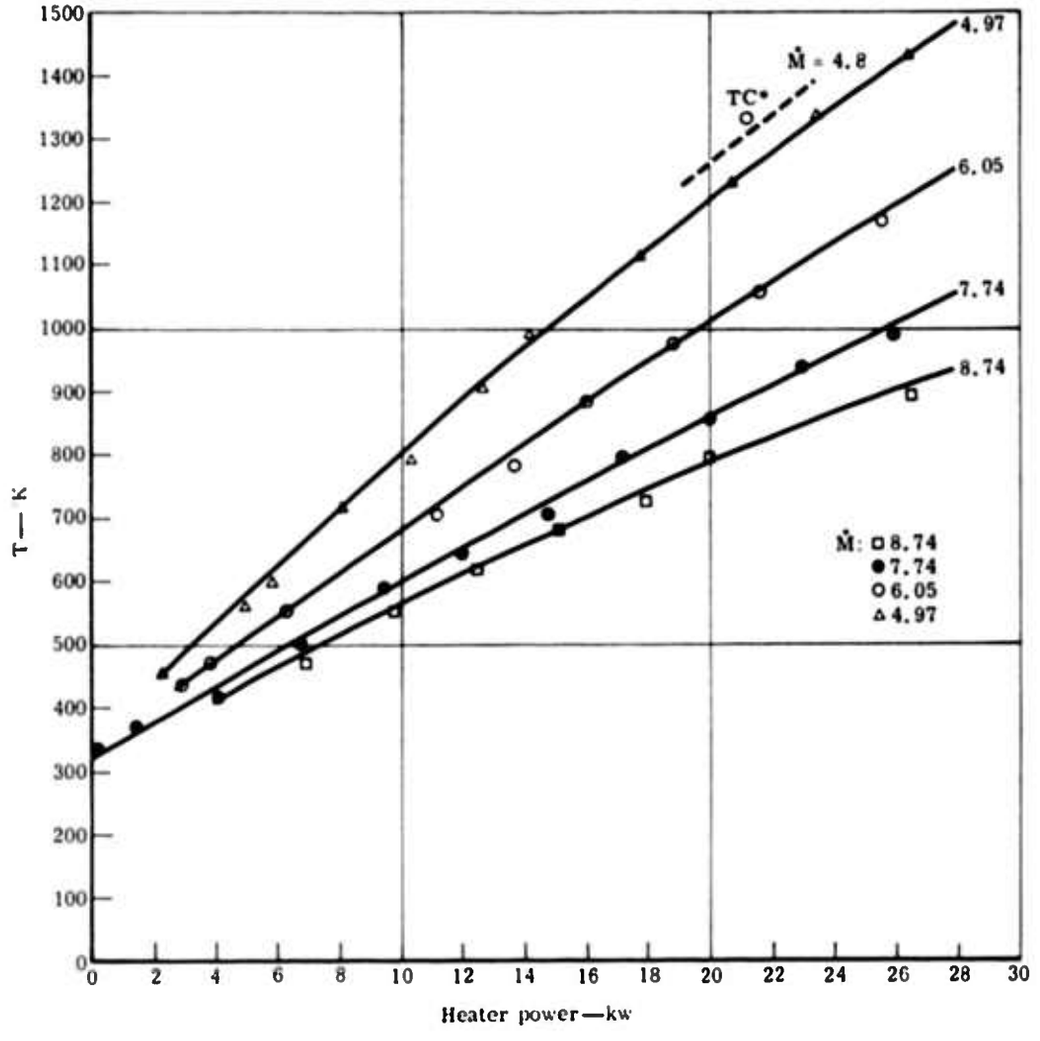


*Temperature measured with Thermocouple, $\dot{M}$ = 4.8

**Figure 11. Gas temperature vs heater power mass flow $\dot{M}$ parameter**

Figure 14 shows the helium jet in the test section. The electrodes were separated sufficiently to show the jet. For running purposes, electrode distances of 1 cm and 2 cm were used.

For shakedown purposes, the electrodes were connected to a variable load resistor and output voltage and current were measured. For runs with pure helium, of course, there should be no output at all. However, a small output voltate in the order of 0.2 v and a small output current in the order of 0.3 ma were detected. The exact values depend strongly on voltage of the heater, mass flow, and gas temperature, and only slightly on the magnetic field. This

indicated that the observed output was due to a leakage current from the heater coming either through the gas or along walls. If it is a leakage current through the gas, its value may be increased tremendously when injecting cesium. This fact has to be borne in mind when one is interpreting data from power runs at low power levels.

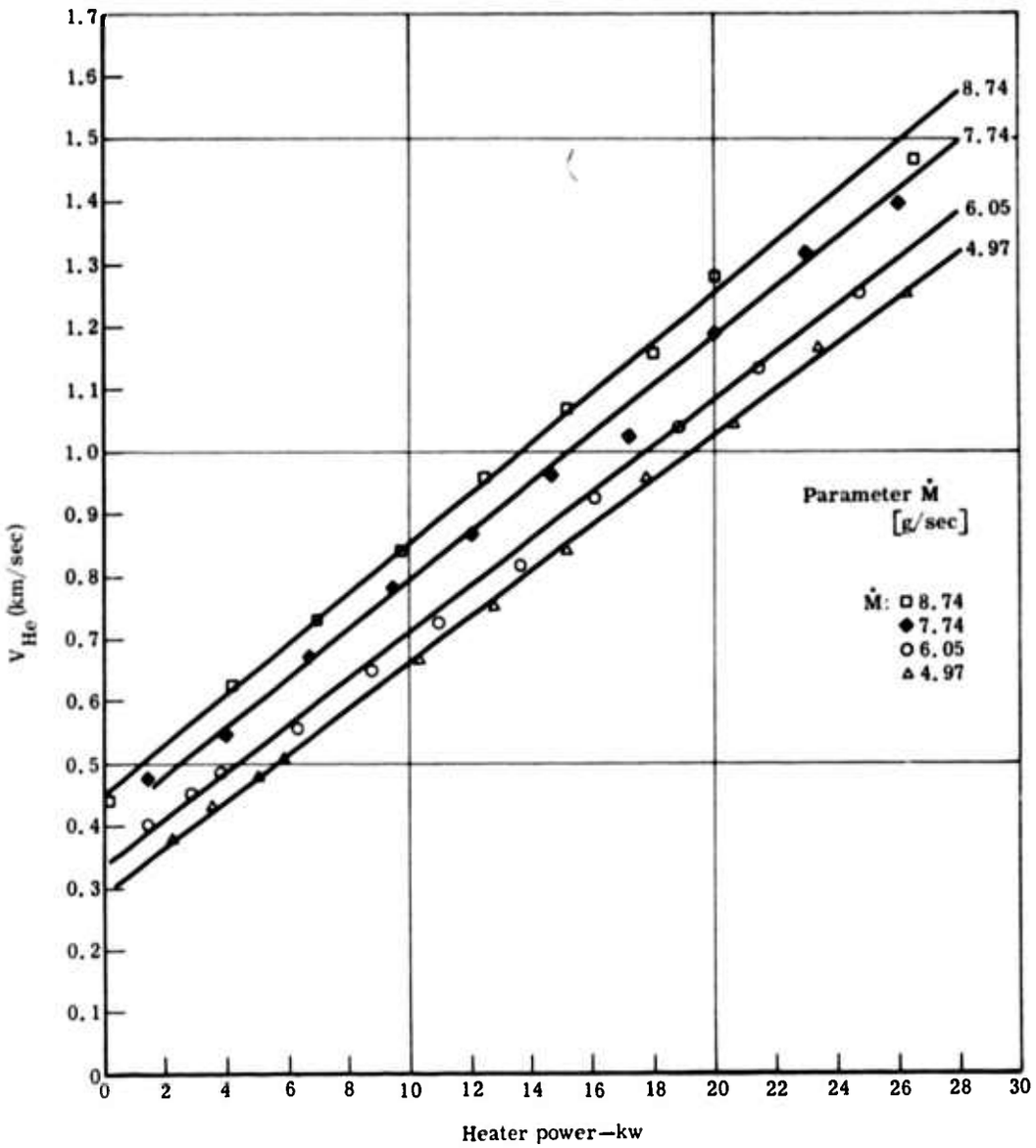


Figure 12. Gas velocity vs heater power

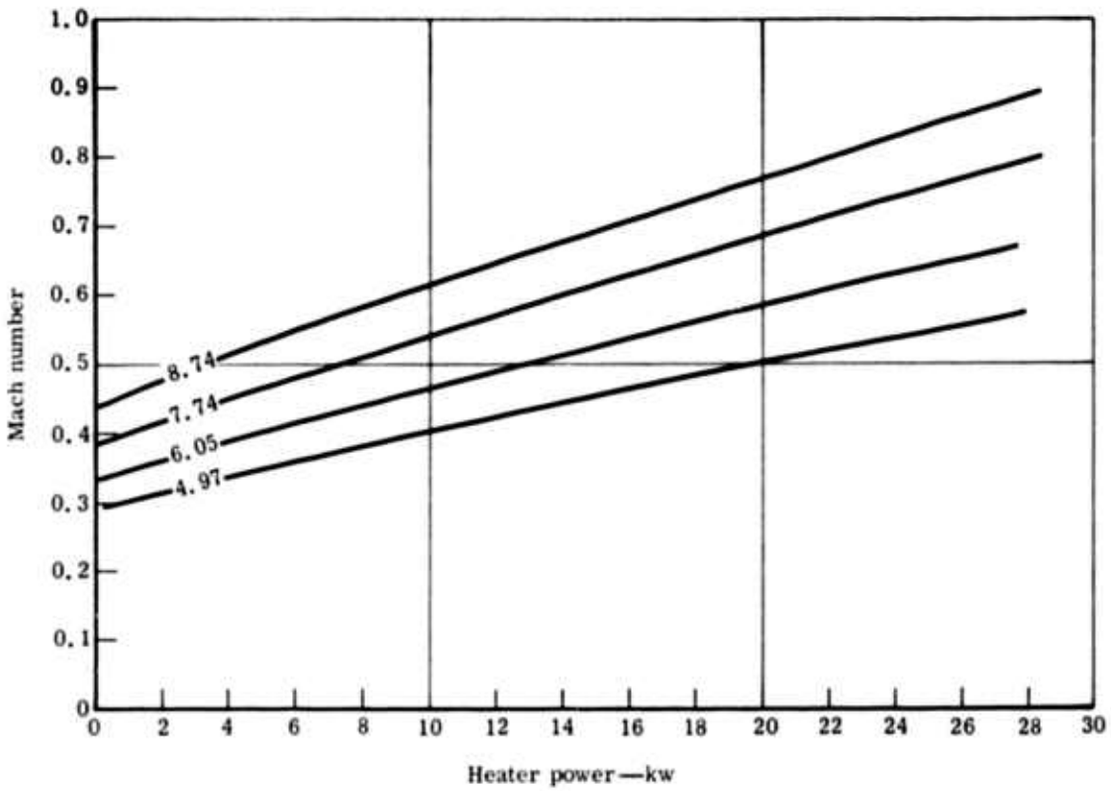


**Figure 13. Mach number vs heater power mass flow $\dot{M}$ parameter (g/sec)**

A more extensive investigation of this phenomenon is scheduled and the results will be included in the next Quarterly Summary report.

RUNS WITH HELIUM SEEDED WITH CESIUM

The objective of the first runs with the seeded working fluid was to learn more about the problems that are involved in the operation of this type of loop. Major points of concern were:

- Material attack of the tantalum structure
- Material attack of the ceramic structure
- Possible arcing of the heater
- Performance of the cesium injection system
- Performance of the cesium separation and seed recovery

**Figure 14. Helium jet in test section.**

Besides this, the electrical data, even if preliminary and crude, give the most important information. It allows the design of the proper instrumentation setup and defines the problems which are involved.

The preliminary conclusions, drawn from these runs were:

- The system is still operational; therefore, only minor design modifications are necessary due to the experience obtained from these runs.
- Only minor arcing did occur within the heater.
- A judgment on material attack can be made only after disassembly of the system.

The cesium injection system has to be improved. Also, the use of a two-stage separator instead of the present one-stage separator is desirable. The quartz window devitrified due to the cesium attack and should be replaced with sapphire windows. These changes will be made as soon as the present series of runs is completed.

With the present setup the generated voltage and the leakage voltage are of opposite polarity. Therefore, values of 1.0 volt and 0.4 ma at 1000°K gas temperature, reported in Section II, are pessimistic values.

After learning more about the leakage mechanism and after more runs are made with reversed magnetic field, it will be possible to give a definite value of the generated power at 1000°K gas temperature.

## V. THEORETICAL INVESTIGATIONS

### IONIZATION EQUILIBRIUM OF PLASMA IN MAGNETIC FIELD

#### Thermodynamic Equilibrium in Plasma

A plasma can be only in true thermodynamic equilibrium if it is homogeneous and if escape of radiation is negligible. Consequently, in presence of a magnetic field spatial constancy of this field must be demanded. Inhomogeneity or existence of different temperatures in the components is necessarily connected with irreversible processes like diffusion, heat conduction, and electrical conduction, which disturb the thermodynamic equilibrium. It is obvious that the equilibrium state is an ideal limit to which an actual plasma can only approximate.

The reactions occurring in a plasma are provided by inelastic particle collisons. As known from statistical mechanics, the contribution of these interactions to the total energy can be neglected when the system is sufficiently dilute. In the Hamilton operator of the plasma system,

$$H_{Total} = \sum_{j=1}^{N} \frac{\left(\vec{P}_j - e_j \vec{A}\right)^2}{2 m_j} + \frac{1}{2} \sum_{j=1}^{N} \sum_{k=1}^{N} W\left(\left|\vec{r}_j - \vec{r}_k\right|\right) - \sum_{j} \vec{\mu}_j \cdot \vec{B} \qquad (1)$$

where

$\vec{P}_j$ = generalized momentum operator of the j-th particle

$e_j$, $m_j$ = charge and mass of the j-th particle

$W\left(\left|\vec{r}_j - \vec{r}_k\right|\right)$ = interaction energy for the j-th and k-th particle

$\vec{\mu}_j$ = magnetic moment of the j-th particle

$\vec{A}$ = vector potential of the magnetic field $\vec{B}$

therefore, the interaction energies, W, of the particles are disregarded. As a consequence, the result of the investigation is independent of the laws of interaction.

The subject of the investigation is a homogeneous plasma submerged into a constant magnetic field in which ionization and deionization reactions take place on the average at the same rate:

$$a \rightleftharpoons i + e, \qquad \begin{matrix} a = \text{atoms} \\ e = \text{electrons} \\ i = \text{ions} \end{matrix} \tag{2}$$

The condition for thermodynamic equilibrium, formulated in terms of the electrochemical potentials, $\mu_r$, of the components r, is

$$\sum_r \nu_r \mu_r = 0, \text{ i.e., } \mu_e + \mu_i - \mu_a = 0 \tag{3}$$

With $Z_r$ as the sume of states and $N_r$ as total number of particles of the r - component, the potentials, $\mu_r$, are given by

$$\mu_r = - k T \left[ \frac{\partial \ln Z_r}{\partial N_r} \right]_{\vec{B},\ T,\ V,\ N_{r \neq s}} \tag{4}$$

The sum of states is conveniently expressed by the collective of the energy eigenvalues, $E_a$, which a representative particle of the s-component can exhibit:[1*]

$$Z_r = \frac{1}{N_r!} \left[ \sum_a e^{-E_a / k T} \right]^{N_r} \tag{5}$$

This relation refers to weakly interacting particles of Bose and Fermi types.

Sum of States for Particles in Magnetic Field

As a theoretical model, consider a plasma box, Figure 15, of side lengths $S_x$, $S_y$, $S_z$ which contains $N_e$ electrons, $N_i$ ions, and $N_a$ atoms in homogeneous mixture. The magnetic field, $\vec{B}$, is assumed to be directed along the z-axis. It is given in terms of the vector potential by:

$$\vec{B} = \nabla \times \vec{A} = e_z \left( - \frac{A_x}{y} \right), \quad \begin{matrix} A_y \\ A_z \end{matrix} = 0 \tag{6}$$

* Superscripts denote references listed in Section VI.

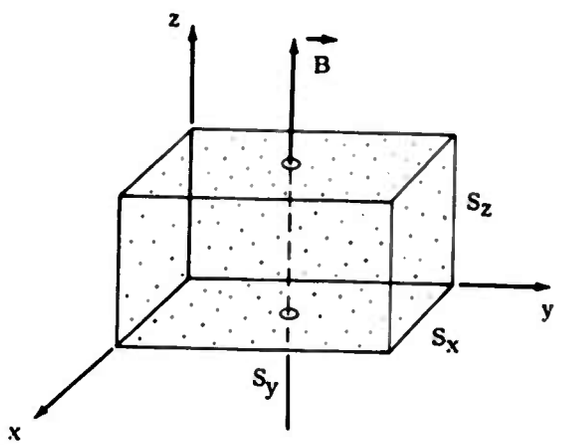


**Figure 15. Plasma box with magnetic field.**

The plasma is treated in the semiclassical approximation which is based on the assumption[2]

$$\frac{N_r}{V}\left(\frac{2\pi m_r k T}{h^2}\right)^{-3/2} \ll 1, \quad r = e, i, a \tag{7}$$

Electron Component

The magnetic moment of the electrons due to the spin is $\vec{\mu} = \vec{\sigma}\, e\hbar/m_e$ ($\sigma = -\frac{1}{2}, +\frac{1}{2}$), where $e > 0$ is the elementary charge. As the spin operator, $\boldsymbol{\sigma}$, commutes with the Hamilton operator, $\mathbf{H}$, and the constant vector potential, $\vec{A}$, commutes with the momentum operator, $\vec{P}$, the wave equation of the electrons can be derived as:

$$\left[\frac{1}{2} m_e \left(\frac{e B}{m_e}\right)^2 \left(y + \frac{P_x}{e B}\right)^2 + \frac{P_y^2 + P_z^2}{2 m_e} - \sigma \hbar \frac{e B}{m_e}\right] \psi = E \psi \tag{8}$$

The wave function is obviously of the form

$$\psi = \text{Const} \times e^{\frac{i}{\hbar}(P_x x + P_z z)} \times u(y)$$

where $P_x$, $P_y$ are momentum eigenvalues, $-\infty < P_x, P_y < +\infty$. Separation of the coordinates leads to

$$\frac{d^2u}{dy^2} + \frac{2m_e}{\hbar^2}\left[E + \sigma\hbar\frac{eB}{m_e} - \frac{P_z^2}{2m_e} - \frac{1}{2}m_e\left(\frac{eB}{m_e}\right)^2\left(y + \frac{P_x}{eB}\right)^2\right]u = 0 \qquad (9)$$

Equation (9) corresponds to the wave equation for a linear oscillator of energy, $E_{osc} = E + \sigma\hbar\frac{eB}{m_e} - \frac{P_z^2}{2m_e}$, oscillating with the electron gyration frequency, $\omega_e^B = eB/m_e$, about the point $y_o = -P_x/eB$. Accordingly, the energy eigenvalues are[3]

$$E_{\nu, P_z, \sigma} = \left(\nu + \frac{1}{2}\right)\hbar\frac{eB}{m_e} - \sigma\hbar\frac{eB}{m_e} + \frac{P_z^2}{2m_e}, \quad \nu = 0, 1, 2, \ldots \qquad (10)$$

The momentum eigenvalues $P_x$ and $P_z$ in Equations (9) and (10) are still continuously degenerate. This degeneracy is readily removed upon considering the finite dimensions of the box. It results for the number of momentum eigenvalues in the phase space element $\Delta P_x L_x \cdot \Delta P_z L_z$,

$$\Delta\xi = \frac{\Delta P_x L_x}{2\pi\hbar} \cdot \frac{\Delta P_z L_z}{2\pi\hbar} \qquad (11)$$

From the condition that the gyration centers must be contained within the limits $0 \le y \le L_y$, namely $0 \le y_o \le L_y$, it follows $\Delta P_x = eBL_y$. Consequently, the number of momentum eigenvalues in the considered phase space element becomes[4]

$$\Delta\xi = \frac{V}{(2\pi\hbar)^2} eB\Delta P_z, \quad V \equiv S_x S_y S_z \qquad (12)$$

By extending the dimensions of the box to infinity, and considering Equations (10) and (12), it follows for the electron component:

$$\sum_{a} e^{-E_a/k\,T} \rightarrow \frac{V\,e\,B}{(2\pi\hbar)^2} \int_{-\infty}^{\infty} e^{-P_z^2/2\,m_e\,k\,T}\, d\,P_z \times \sum_{\nu=0}^{\infty} e^{-\left(\nu+\frac{1}{2}\right)\hbar\frac{e\,B}{m_e\,k\,T}} \times \sum_{\sigma=-1/2}^{+1/2} e^{-\sigma\hbar\frac{e\,B}{m_e\,k\,T}} \tag{13}$$

(The double spin degeneracy is removed here by the magnetic field.) After evaluating the integral, the sum of states is obtained in the form:

$$Z_c = \frac{1}{N_e!}\left[\frac{V\,e\,B}{(2\pi\hbar)^2}\sqrt{2\pi m_e\,k\,T}\sum_{\nu=0}^{\infty} e^{-\left(\nu+\frac{1}{2}\right)\hbar\frac{e\,B}{m_e\,k\,T}} \sum_{\sigma=-1/2}^{+1/2} e^{-\sigma\hbar\frac{e\,B}{m_e k\,T}}\right]^{N_e} \tag{14}$$

By means of Stirling's formula, it follows for the chemical potential:

$$\mu_e = -\,k\,T\left\{\ln\left[\frac{e\,B}{(2\pi\hbar)^2}\sqrt{2\pi m_e\,k\,T}\,\frac{V}{N_e}\right] + \ln\sum_{\nu=0}^{\infty} e^{-\left(\nu+\frac{1}{2}\right)\hbar\frac{e\,B}{m_e\,k\,T}} + \ln\sum_{\sigma=-1/2}^{+1/2} e^{-\sigma\hbar\frac{e\,B}{m_e\,k\,T}}\right\} \tag{15}$$

Equations (14) and (15) are valid for plasmas in which a physically well defined electron gyration about the magnetic field exists. This is to be expected when the mean free path $\ell_e = \left[\sum_{r=e,i,a} n_r\,Q_r\right]^{-1}$ is large compared to the gyration radius $r_e = \sqrt{m_e\,k\,T}\,/e\,B$ of the electrons,

$$\ell_e \gg r_e\,. \tag{16}$$

Equivalent to this condition is the demand for the collision frequency to be small compared to the gyration frequency of the electrons,

$$\omega_e^{coll} \ll \omega_e^B \tag{17}$$

where $\omega_e^{coll} = \ell_e^{-1}\sqrt{\frac{k\,T}{m_e}}$ and $\omega_e^B = e\,B/m_e$. The case of strong collisional perturbation of the electron gyration motion is not regarded here.

Ion and Atom Component

Additional energy states due to excitation appear in the ionic and atomic component. The intrinsic energy $E_s$ of a particle with an electronic structure in state s is determined by the four quantum numbers $n_s$, $L_s$, $S_s$, $J_s$, when external fields are absent. In the considered magnetic field, the ion or atom exhibits in each state s due to the quantized orientation of its magnetic moment, $\mu(s) = Mg_s\,(e\hbar/2\,m_e)$—in a statistical sense—the orientational energy eigenvalues $-M\,\mu(s)$, where $M = -J_s, \ldots, +J_s$. The nontranslational energy eigenvalues of the considered particles are, therefore,

$$E_{M,\,s} = E_s - Mg_s\frac{e\hbar}{2\,m_e}\,B \tag{18}$$

It is assumed here that the spin-orbit interaction is predominant. The Landé splitting factor is defined by

$$g_s = 1 + \frac{J_s\,(J_s+1) + S_s\,(S_s+1) - L_s\,(L_s+1)}{2\,J_s\,(J_s+1)} \tag{19}$$

It is usual to write $E_s$ as the sum of the energy of the atom in ground state, $\epsilon_o$, and the excitation energy of the s-th state, $\kappa_s$,

$$E_s = \epsilon_o + \kappa_s, \quad \kappa_o \equiv 0 \tag{20}$$

By consideration of Equations (18), (19), and (20), the sum of state and chemical potential of the ions is easily derived in analogy to the previous case. As the ion gyration radius $r_i = \sqrt{m_i\,k\,T}\,/e\,B$ is $\sqrt{m_i/m_e}$ times larger than the electron gyration radius, two situations are of interest:

1. Unperturbed Ion Gyration Motion

Ion gyration radius $r_i \ll$ ion mean free path $\ell_i$. It results:

$$Z_i = \frac{1}{N_i!}\left[\frac{e\,B\,V}{(2\pi\hbar)^2}\sqrt{2\pi m_i\,k\,T}\sum_{\nu=0}^{\infty} e^{-\left(\nu+\frac{1}{2}\right)\hbar\frac{e\,B}{m_i\,k\,T}} \times e^{-\epsilon_o^i/k\,T}\sum_{M=-J_s^i}^{+J_s^i}\sum_{s=0}^{\infty} e^{-\left(\kappa_s^i - Mg_s^i\,\hbar\frac{e\,B}{2\,m_e}\right)/\,k\,T}\right]^{N_i} \tag{21}$$

$$\mu_i = -\,k\,T\left\{\ln\left[\frac{e\,B}{(2\pi\hbar)^2}\sqrt{2\pi m_i\,k\,T}\,\frac{V}{N_i}\right] + \ln\sum_{\nu=0}^{\infty} e^{-\left(\nu+\frac{1}{2}\right)\hbar\frac{e\,B}{m_i\,k\,T}} - \frac{\epsilon_o^i}{k\,T} + \ln\sum_{M=-J_s^i}^{+J_s^i}\sum_{s=0}^{\infty} e^{-\left(\kappa_s^i - Mg_s^i\,\hbar\frac{e\,B}{2\,m_e}\right)/k\,T}\right\} \tag{22}$$

2. Perturbed Ion Gyration Motion:

Ion gyration radius $r_i \gg$ ion mean free path $\ell_i$. It results:

$$Z_i = \frac{1}{N_i!}\left[\left(\frac{2\pi m_i\,k\,T}{h^2}\right)^{3/2} V \times e^{-\epsilon_o^i/k\,T}\sum_{M=-J_s^i}^{+J_s^i}\sum_{s=0}^{\infty} e^{-\left(\kappa_s^i - Mg_s^i\,\hbar\frac{e\,B}{2\,m_e}\right)/k\,T}\right]^{N_i} \tag{23}$$

$$\mu_i = -\,k\,T\left\{\ln\left[\left(\frac{2\pi m_i\,k\,T}{h^2}\right)^{3/2}\frac{V}{N_i}\right] - \frac{\epsilon_o^i}{k\,T} + \ln\sum_{M=-J_s^i}^{+J_s^i}\sum_{s=0}^{\infty} e^{-\left(\kappa_s^i - Mg_s^i\,\hbar\frac{e\,B}{2\,m_e}\right)/k\,T}\right\} \tag{24}$$

Formally, Equation (23) can be derived by carrying through the limit $B \to 0$ in the translational part of Equation (21).

An expression similar to Equation (23) is valid for uncharged particles, as their translational energy states are unaffected by the magnetic field. The corresponding expressions for the sum of states and chemical potential of the neutral atom component are:

$$Z_a = \frac{1}{N_a!}\left[\left(\frac{2\pi m_a k T}{h^2}\right)^{3/2} \frac{V}{N_a} \times e^{-\epsilon_o^a/k T} \sum_{M=-J_s^a}^{+J_s^a} \sum_{s=0}^{\infty} e^{-\left(\kappa_s^a - M g_s^a \hbar \frac{e B}{2 m_e}\right)/k T}\right]^{N_a} \quad (25)$$

$$\mu_a = - k T \left\{ \ln\left[\left(\frac{2\pi m_a k T}{h^2}\right)^{3/2} \frac{V}{N_a}\right] - \frac{\epsilon_o^a}{k T} + \ln \sum_{M=-J_s^a}^{+J_s^a} \sum_{s=0}^{\infty} e^{-\left(\kappa_s^a - M g_s^a \hbar \frac{e B}{2 m_e}\right)/k T} \right\} \quad (26)$$

The double sums in Equations (21) through (26) are later designated by $u_r(B, T)$ (excitational partition function of the component r, r = i, a).

Ionization Equations for Plasma in Magnetic Field

The equilibrium particle composition of plasma in magnetic field is readily obtainable by inserting the applying chemical potentials into the condition for thermodynamic equilibrium, Equation (3). Again, the following cases are considered:

1. Unperturbed Electron and Ion Gyration:

From Equation (3) and Equations (15), (22), and (26), it follows as ionization equation:

$$\frac{n_e n_i}{n_a} = h^3 \frac{\sqrt{2\pi m_e}\sqrt{2\pi m_i}}{(2\pi m_a)^{3/2}} \left[\frac{e B}{(2\pi\hbar)^2}\right]^2 \sum_{\nu=0}^{\infty} e^{-\left(\nu+\frac{1}{2}\right)\frac{\hbar e B}{m_e k T}} \sum_{\nu=0}^{\infty} e^{-\left(\nu+\frac{1}{2}\right)\frac{\hbar e B}{m_i k T}} \times$$

$$\sum_{\sigma=-1/2}^{+1/2} e^{-\sigma \frac{\hbar e B}{m_e k T}} \frac{u_B^i(T)}{u_B^a(T)} (k T)^{-1/2} e^{-\frac{(\epsilon_o^i - \epsilon_o^a)}{k T}} \quad (27)$$

2. Unperturbed Electron Gyration, Perturbed Ion Gyration:

From Equation (3) and Equations (15), (24), and (26), it follows as ionization equation:

$$\frac{n_e\, n_i}{n_a} = h^{3/2}\sqrt{2\pi m_e}\left(\frac{m_i}{m_a}\right)^{3/2}\frac{e\,B}{(2\pi\hbar)^2}\sum_{\nu=0}^{\infty} e^{-\left(\nu+\frac{1}{2}\right)\frac{\hbar e\,B}{m_e\,k\,T}}\sum_{\sigma=-1/2}^{+1/2} e^{-\sigma\frac{\hbar e\,B}{m_e\,k\,T}}\times$$

$$\frac{u_B^i(T)}{u_B^a(T)}\,(k\,T)^{+1/2}\; e^{-\frac{(\epsilon_o^i-\epsilon_o^a)}{k\,T}} \qquad (28)$$

The particle densities $n_r$ are defined by $n_r = N_r/V$, $r = e, i, a$. The difference of the energies of the ion and atom in ground state, $\epsilon_o^i - \epsilon_o^a$, has the physical meaning of the ionization energy. The derived ionization equations refer to plasmas with negligible interaction energy of the particles.

Consequences

For discussion, it is suitable to replace the infinite geometric series appearing in the ionization formulae, Equations (27) and (28), as follows:

$$\sum_{\nu=0}^{\infty} e^{-(\nu+1/2)\frac{\hbar e\,B}{m_r\,k\,T}} = \left[e^{+\frac{\hbar e\,B}{2\,m_r\,k\,T}} - e^{-\frac{\hbar e\,B}{2\,m_r\,k\,T}}\right]^{-1}, \qquad r = e,\ i \qquad (29)$$

In order to reveal first the relation with existing theory, regard the limits:

i) $$\lim_{B\to 0} h^{3/2}\sqrt{2\pi m_r}\,\frac{e\,B}{(2\pi\hbar)^2}\sum_{\nu=0}^{\infty} e^{-(\nu+1/2)\frac{\hbar e\,B}{m_r\,k\,T}} = \left(\frac{2\pi m_r}{h}\right)^{3/2} k\,T,\quad r = e, i$$

$$\text{j)} \quad \lim_{B \to 0} \sum_{\sigma = -1/2}^{+1/2} e^{-\sigma \frac{\hbar e B}{m_e k T}} = 2$$

$$\text{k)} \quad \lim_{B \to 0} u_B^r(T) = \sum_{s=0}^{\infty} \left(2J_s^r + 1\right) e^{-\epsilon_s^r / k T} = u_o^r(T), \quad r = i, a$$

The limit j demonstrates the double degeneracy of the electrons and the limit k the $(2J_s^r + 1)$—times degeneracy of the ionic and atomic electron states in absence of the field, $B = 0$.

By consideration of limits i through k, both Equations (27) and (28) yield in the limit of vanishing field, $B \to 0$:

$$\frac{n_e\, n_i}{n_a} = 2\left(\frac{2\pi m_e}{h^2}\right)^{3/2} \frac{u_o^i(T)}{u_o^a(T)} (k T)^{3/2} e^{-\frac{(\epsilon_o^i - \epsilon_o^a)}{k T}} \tag{30}$$

This is the well known Eggert-Saha equation, describing the ionization equilibrium of field-free plasmas.

It is immediately relevant that the ionizational composition of plasma in magnetic field deviates from the Eggert-Saha equilibrium only at high magnetic field intensities, when the quanta of the electron gyration motion, $\hbar \omega_e = \hbar \frac{e B}{m_e}$, are of the order of magnitude of the thermal energy:

$$\frac{\hbar \omega_e}{k T} \gtrapprox 1 \tag{31}$$

In this case, the magnetic field has the effect of remarkably increasing the degree of ionization. The condition of Equation (31) can be realized by means of high intensity short-time electromagnets in low temperature plasmas. Under these extreme conditions, the spin-orbit interaction energy in the atom can be small compared to the energy of the atomic magnetic moment in the exterior field. In this situation, the so-called Paschen-Bach effect is observed. This phenomenon influences somewhat the form of the excitational partition functions as defined in Equations (24) and (26).

It can be presumed that the quanta of the ion gyration motion, $\hbar\omega_i = \hbar\frac{e\,B}{m_i}$, are small compared to the thermal energy, kT, at all technically achievable field intensities. Furthermore, as the influence of the magnetic field is of interest only at low temperatures, the ions and atoms can be considered to be in their ground state. It follows from Equation (27) or (28):

$$\frac{n_e\, n_i}{n_a} = \sqrt{2\pi m_e}\,\frac{e\,B}{(2\pi\hbar)^2}\,\mathrm{ctgh}\left[\frac{\hbar\, e\, B}{2\, m_e\, k\, T}\right]\frac{u_B^i\,(M_o)}{u_B^a\,(M_o)} \times (k\,T)^{1/2}\, e^{-\frac{\epsilon_o^i - \epsilon_o^a}{k\,T}} \qquad (32)$$

where the hyperbolic contangent has been introduced. Furthermore, $u_B^a\,(M_o)$ and $u_B^i\,(M_o)$ designate the orientational partition function of the atoms and ions in ground state, respectively. These are obtained from the corresponding excitational partition functions by taking, in the infinite series over s, only the first term (s = 0). When Russell-Saunders coupling does not apply, the partition functions have to be modified appropriately.

Disregarding nonequilibrium effects, the ionization degree in MPD converter plasmas can be calculated—in a very rough approximation—from equilibrium theory. For the usual region of temperature (1000-3000°K) and magnetic field intensity ( 10 - 20 $\times 10^3$ gauss) in converter systems, the Eggert-Saha equation and the new ionization equation, Equation (32), lead to practically the same result.

## QUASI-KINETIC THEORY OF REACTING PLASMA

A theoretical description of multicomponent converter plasmas should include that the individual components are not in thermal equilibrium with each other, and that this intercomponent nonequilibrium also depends strongly on the inelastic particle collisons. The thermal nonequilibrium among the components is due to the fact that because of the large mass differences of the different particles, approximate equilibrium in the single component is much more easily achieved than between the light and heavy particle components. The possible nonequilibrium to be observed in stationary state is determined primarily by the mechanism of electrical energy input, the distributive intercomponent convective processes, and the reactive particle flux and reactive energy flux sources.

# Allison

A kinetic theory for multitemperature plasmas based on the Boltzmann equation has been given by Schrade[5] and was later reconsidered in more detail by Schindler[6]. This theory is extended in the following paragraphs to reacting converter plasmas in a classical approach neglecting the perturbation of the particle distribution functions by the reactions. In this connection it is remarkable that in an actual plasma these perturbations are presumably smoothed in the region above the thermal velocity by microinstabilities.

## Theoretical Method

Designate by $\vec{w}_s = \vec{v}_s - \bar{\vec{v}}_s$ the actual particle velocity of the s-component as observed in a system moving with the mean mass velocity, $\bar{\vec{v}}_s$, of the s-component. In the individual frame of reference of the s-component, the n-th order velocity moment of the s-component is then defined by

$$M^{(n)}_{s,ij\ldots} = m_s \int w_{s,i}\, w_{s,j} \ldots f_s(\vec{v}_s, \vec{r}, t) \cdot d\vec{v}_s \tag{33}$$

The first thirteen scalar velocity moments, which have a simple physical meaning, are:

| | |
|---|---|
| Mass density: | $n_s m_s = m_s \int f_s \, d\vec{v}_s$ |
| Mass current: | $j_{s,i} = m_s \int w_{s,i} f_s \, d\vec{v}_s$ |
| Pressure tensor: | $P_{s,ij} = m_s \int w_{s,i} w_{s,j} f_s \, d\vec{v}_s$ |
| Heat current vector: | $2\vec{q}_{s,i} = m_s \int w_s^2 w_{s,i} f_s \, d\vec{v}_s$ |

Scalar pressure, $p_s$, and thermal energy density, $U_s$, are defined by the reduced second order velocity moment:

$$p_s = m_s \int w_s^2 f_s \, d\vec{v}_s = \frac{2}{3} U_s$$

By multiplication of Boltzmann's Equation with the tensor $m_s w^{(n)}_{s,ij\ldots} = m_s w_{s,i} w_{s,j} \cdots$ and subsequent integration with respect to velocity space, it can be shown that the n-th order velocity moments satisfy the general equation of change (summation according to Einstein convention),

$$\frac{\partial}{\partial t} M^{(n)}_{s,ij\ldots} + \frac{\partial}{\partial r_l}\left[\bar{v}_{s,l} M^{(n)}_{s,ij\ldots} + M^{(n+1)}_{s,lij\ldots}\right] +$$

$$\sum_a \left[ M^{(n-1)}_{s,i\ldots \neq a} \frac{\partial \bar{v}_{s,a}}{\partial t} + M^{(n-1)}_{s,i\ldots \neq a} \bar{v}_{s,l} \frac{\partial v_{s,a}}{\partial r_l} + M^{(n)}_{s,li\ldots \neq a} \frac{\partial v_{s,a}}{\partial r_l} \right] -$$

$$\frac{e_s}{m_s} \sum_a \left[ E_a + \epsilon_{a\lambda\mu} \bar{v}_{s,\lambda} B_\mu \right] \sum_m M^{(n-1)}_{s,i\ldots \neq m} \delta_{am} - \tag{34}$$

$$\frac{e_s}{m_s} \sum_a \epsilon_{a\lambda\mu} B_\mu \sum_m M^{(n)}_{s,\lambda i\ldots \neq m} \delta_{am} =$$

$$m_s \sum_r \int w_{s,i}\, w_{s,j} \cdots \left[\frac{d f_s}{dt}\right]^{\text{elastic}}_r \cdot d\vec{v}_s +$$

$$m_s \sum_{(r,\rho,\ldots)} \int w_{s,i}\, w_{s,j} \cdots \left[\frac{d f_s}{dt}\right]^{\text{reactive}}_{(r,\rho\ldots)} \cdot d\vec{v}_s$$

The expressions on the right side of Equation (34) represent the collision integrals for elastic and reactive collisons, respectively.

The elastic particle collisions are treated exclusively as two-body collisions. For elastic two-body interactions, the collisional change of the distribution function is given by[7]

$$\left[\frac{d f_s}{dt}\right]^{\text{elastic}}_r = \iiint \left[f_s' f_r' - f_s f_r\right] \sigma_{sr} \left|\vec{v}_r - v_s\right| d\Omega\, d\vec{v}_r \tag{35}$$

The reactive many-body collision integrals are treated in a phenomenological way by introducing reaction velocities.

Neglecting the influence of the reactive collisions, the velocity distribution functions of the components s are given in the so-called 13-moment-approximation by[8]

$$f_s = n_s \left(\frac{m_s}{2\pi k T_s}\right)^{3/2} \exp\left(-\frac{m_s w_s^2}{2 k T_s}\right) \times \left[1 + \frac{m_s}{2 k T_s}\left(\frac{P_{s,ij}}{p_s} - \delta_{ij}\right) w_{s,i} w_{s,j} + \frac{m_s}{k T_s p_s}\left(\frac{m_s w_s^2}{5 k T_s} - 1\right) q_{s,i} w_{s,i}\right] \quad (36)$$

From Equation (34), the field and transport equations for the s-components are obtained as momentum conservation equations.

The elastic collision integrals in the momentum conservation equations can be readily evaluated by means of Equation (36) for the following models:

- Interaction corresponding to rigid elastic spheres of radii $r_s$ and $r_r$ for encounters between a neutral and another neutral particle, or between a charged and a neutral particle. In the center of mass system of the colliding particles, the differential cross section is

$$\sigma_{sr} = \frac{1}{4}(r_s + r_r)^2 \quad (37)$$

In evaluating the collision integrals, Equation (37) leads to a total transport cross section (Ramsauer cross section)[7]

$$Q_{sr} = \pi (r_s + r_r)^2 \quad (38)$$

- Interactions corresponding to Coulomb scattering fields for encounters between particles of charge $e_s$ and $e_r$, where the collision parameter is cut off at the Debye shielding distance,

$$D = \left[\frac{4\pi}{k}\left(\frac{n_e e_e^2}{T_e} + \frac{n_i e_i^2}{T_i}\right)\right]^{-1/2}$$

In the center of mass system of the colliding particles, the differential cross section is

$$\sigma_{sr} = \left[\frac{e_s e_r}{2\mu_{sr}(\vec{v}_s - \vec{v}_r)^2}\right] \sin^{-4}\frac{\kappa}{2} \quad (39)$$

In evaluating the collision integrals, Equation (39) leads to a total mean transport cross section (Grosdover cross section)[7]

$$Q_{sr} = \frac{\pi}{4}\left[\frac{e_s\, e_r}{k\, T_{sr}}\right]^2 \ln\theta_{sr}\,,\ \theta_{sr} \gg 1 + \left[\frac{6\, k\, T_{sr}\, D}{e_s\, e_r}\right]^2 \tag{40}$$

The reduced mass, $\mu_{sr}$, and reduced temperature, $T_{sr}$, are defined by

$$\mu_{sr} = \frac{m_s\, m_r}{m_s + m_r}\,,\quad T_{sr} = \mu_{sr}\left(\frac{T_s}{m_s} + \frac{T_r}{m_r}\right) \tag{41}$$

As reactions, ionization and recombination processes are considered. It is assumed that the ionization of the neutral atoms is provided by electron collisions, and the recombination of the ions is due to three-body electron-ion-electron collisions. The corresponding reaction equation is

$$e + a \rightleftarrows i + e + e \tag{42}$$

This model applies, in particular, to the situation prevailing in low temperature ($T \leq 3000°K$) alkali seeded (seeding ratio $\epsilon \cong 10^{-2}$) noble gas plasmas of atmospheric pressure. In specifying this type of plasma, the following indices are introduced:

Index o: for noble gas atoms
Index a: for neutral seeding atoms
Index i: for ionic seeding atoms
Index e: for electrons

In the considered temperature range, the noble gas component is treated as nonreacting.

The zero order reactive collision integrals represent the reactive mass production of the species s. For the regarded reactions, introduce $\Gamma^+$ as ionization reaction velocity and $\Gamma^-$ as recombination reaction velocity. According to the definition of reaction velocities, the following relations can be established:

$$m_s \sum_{(r,\rho)} \int \left[\frac{d\, f_s}{d\, t}\right]^{\text{reactive}}_{(r,\rho)} \cdot d\vec{v}_s = \nu_s\, m_s\, (\Gamma^+ - \Gamma^-),\ s = e,\ i,\ a,\ o \tag{43}$$

it is for the electron component s = e: $(r, \rho) = (a, o), (i, e)$; and appropriately for the remaining components. The $\nu_s$ designate the stoichiometric coefficients in the reaction equation as formulated in Equation (42):

$$\nu_e = +2 - 1 = +1, \quad \nu_i = +1, \quad \nu_a = -1, \quad \nu_o \equiv 0 \tag{44}$$

It is immediately recognized that summation of Equation (43) with respect to the s-components yields zero (conservation of mass in the reactions).

The total reaction velocity, $\Gamma \equiv \Gamma^+ - \Gamma^-$, is given in terms of the (electron collision) ionization probability coefficient, $S_{ea}$, and (three-body electron-ion-electron) recombination probability coefficient, $R_{eie}$, by

$$\Gamma \equiv \Gamma^+ - \Gamma^- = n_e n_a S_{ea} - n_i n_e^2 R_{eie} \tag{45}$$

The reaction coefficients thus defined are—in first approximation—functions of the electron temperature alone. According to Eiwert[9]:

$$S_{ea} = \frac{3}{2\sqrt{\pi}} \frac{\phi c}{a^3} \zeta_n \left(\frac{k T_e}{\epsilon_n}\right)^{1/2} \left(\frac{\epsilon_n}{\epsilon_{Ii}}\right)^{-3/2} e^{\frac{-\epsilon_n}{k T_e}} G\left(\frac{\epsilon_n}{k T_e}\right) \xi \tag{46}$$

$$R_{eie} = 6\pi \frac{\phi c\, a^3}{a^3} \zeta_n \frac{u_a}{u_i} \left(\frac{\epsilon_n}{k T_e}\right) \left(\frac{\epsilon_n}{\epsilon_H}\right)^{-3} G\left(\frac{\epsilon_n}{k T_e}\right) \xi \tag{47}$$

where the correction function of magnitude of order 1 is given by

$$G\left(\frac{\epsilon_n}{k T_e}\right) = 0.7 \left(\frac{\epsilon_n}{k T_e}\right) \left[1 - \left(\frac{\epsilon_n}{k T_e}\right) e^{\frac{\epsilon_n}{k T_e}} \cdot Ei\left(\frac{\epsilon_n}{k T_e}\right)\right] + 0.3 \tag{48}$$

The symbols in Equations (45) and (46) have the meaning:

$$\phi = \frac{8\pi}{3} \left(\frac{e^2}{m c^2}\right)^2 = 6.6 \times 10^{-25}\ \mathrm{cm}^2 = \text{Thomson scattering cross section}$$

$$\alpha = \frac{2\pi e^2}{h c} = \frac{1}{137} = \text{Sommerfeld fine structure constant}$$

$$c = 2.998 \times 10^{10}\ \frac{\mathrm{cm}}{\mathrm{sec}} = \text{velocity of light in free space}$$

$\zeta_n$ = number of electrons in the highest shell n of the atom in ground state

$\epsilon_n$ = ionization energy of the atoms from n-th shell

$\epsilon_H$ = 13.53 e v = ionization energy of hydrogen atom in ground state

$a = \frac{h^2}{4\pi^2 m_e e^2} = 0.529 \times 10^{-8}$ cm = first Bohr radius of hydrogen atom

$u_i$ = excitational portion function of the ions ($u_i \cong 2 J_o^i + 1$ at low temperatures)

$u_a$ = excitational partition function of the atoms ($u_a \cong 2 J_o^a + 1$ at low temperatures)

$\xi$ = factor taking into account ionization from excited states

It is remarkable that Equations (45) and (46) are derived under the assumption of a Maxwellian electron distribution, and that the recombination reactions are considered to be in equilibrium with the ionization reactions. The use of equilibrium reaction coefficients in the description of substantial nonequilibrium plasmas has to be understood in the sense of an approximation.*

As to the reactive collision integrals for the first order velocity moments, it is assumed that their contribution to the momentum transport in the components is negligible. The reactive collision integrals for the reduced velocity moments of second order, representing the reactive energy production in the s-component, are obviously of the form:

$$\frac{1}{2} m_s \sum_{(r,\rho)} \int w_s^2 \left[\frac{d f_s}{d t}\right]_{(r,\rho)}^{\text{reactive}} \cdot d\vec{v}_s = - \Delta E_s (\Gamma^+ - \Gamma^-), \quad s = e, i, a, o \tag{49}$$

It designates $\Delta E_s$ the reactive variation of energy of the s-particles. In the considered reaction mechanisms, the ionization energy is taken primarily from the electron component; the recombination energy is fed primarily into the electron component. Furthermore, with every transformed s-particle, the energy $\nu_s \frac{3}{2} k T_s$ is liberated in the mean. Consequently,

*According to the present state of theory, reaction velocities for nonequilibrium plasmas are not available.

$$\Delta E_e = \nu_e \left[ \epsilon_n - \frac{3}{2} k T_e \right]$$

$$\Delta E_i = - \nu_i \frac{3}{2} k T_i, \quad \Delta E_a = - \nu_a \frac{3}{2} k T_a \tag{50}$$

$$\Delta E_o \equiv 0$$

Summation of Equation (49) with respect to the s-components yields only zero for $\Gamma^+ = \Gamma^-$, i.e., in the trivial case of thermodynamic equilibrium. In nonequilibrium, therefore, the plasma as a whole exhibits a reactive energy source.

Field Equations

The field equations for the components are obtained by evaluating the general equation of change, Equation (34), for the zero order velocity moment, the first order velocity moment, and the reduced second order velocity moment. The appearing reactive collision integrals are given in Equations (43) and (49). After the explicit calculation of the elastic collision integrals the results can be summarized as follows (s, r = e, i, a, o):

Equations of Mass Conservation:

$$\left[ \frac{\partial}{\partial t} + \vec{\bar{v}}_s \cdot \nabla \right] n_s m_s + n_s m_s \nabla \cdot \vec{\bar{v}}_s = \nu_s m_s (\Gamma^+ - \Gamma^-) \tag{51}$$

Equations of Momentum Conservation:

$$n_s m_s \left[ \frac{\partial}{\partial t} + \vec{\bar{v}}_s \cdot \nabla \right] \vec{\bar{v}}_s + \nabla \cdot \vec{\bar{P}}_s - n_s e_s (\vec{E} + \vec{\bar{v}}_s \times \vec{B}) =$$

$$\frac{8}{3} \sqrt{\frac{2}{\pi}} \sum_{r \neq s} n_s n_r Q_{sr} \sqrt{\mu_{sr} k T_{sr}} (\vec{\bar{v}}_r - \vec{\bar{v}}_s) + \tag{52}$$

$$8 \sqrt{\frac{2}{\pi}} \sum_{r \neq s} a_{sr} n_s n_r Q_{sr} \frac{\mu_{sr}^{3/2}}{\sqrt{k T_{sr}}} \left( \frac{\vec{q}_r}{n_r m_r} - \frac{\vec{q}_s}{n_s m_s} \right)$$

Equations of Energy Conservation:

$$\left[\frac{\partial}{\partial t} + \vec{\bar{v}}_s \cdot \nabla\right] U_s + U_s \nabla \cdot \vec{\bar{v}}_s + \vec{\bar{P}}_s : \nabla \vec{\bar{v}}_s + \nabla \cdot \vec{q}_s = -\Delta E_s (\Gamma^+ - \Gamma^-) +$$

$$8\sqrt{\frac{2}{\pi}} \sum_{r \neq s} n_s n_r Q_{sr} \sqrt{\mu_{sr} k T_{sr}} \frac{k}{m_s + m_r} \left[1 + \beta_{sr} \frac{\mu_{sr} (\vec{\bar{v}}_r - \vec{\bar{v}}_s)^2}{2 k T_{sr}}\right] (T_r - T_s) +$$

$$\frac{8}{3}\sqrt{\frac{2}{\pi}} \sum_{r \neq s} n_s n_r Q_{sr} \frac{\mu_{sr}^{3/2}}{\sqrt{k T_{sr}}} \frac{k T_s}{m_s} (\vec{\bar{v}}_r - \vec{\bar{v}}_s)^2 + \qquad (53)$$

$$8\sqrt{\frac{2}{\pi}} \sum_{r \neq s} \alpha_{sr} n_s n_r Q_{sr} \frac{\mu_{sr}^{3/2}}{\sqrt{k T_{sr}}} \left[\gamma_{sr} \left(\frac{\vec{q}_r}{n_r m_r} - \frac{\vec{q}_s}{n_s m_s}\right) + 3 \frac{\vec{q}_s}{n_s m_s}\right] \cdot (\vec{\bar{v}}_r - \vec{\bar{v}}_s)$$

The single coefficients depend on the law of interaction and are, explicitly, for:

Rigid Sphere Interactions:

$$\alpha_{sr} = +1/15$$

$$\beta_{sr} = +1/3$$

$$\gamma_{sr} = \frac{\mu_{sr}}{m_s}\left(25 \frac{T_s}{T_{sr}} - 21\right)$$

Coulomb Interactions:

$$\alpha_{sr} = -1/5$$

$$\beta_{sr} = -1/3$$

$$\gamma_{sr} = \frac{\mu_{sr}}{m_s}\left(\frac{7 T_s}{3 T_{sr}} + \frac{5}{3}\right)$$

The physical meaning of the expressions on the right side of Equations (51), (52), and (53) is in most cases, from their structures, self-relevant. In Equation (51), the terms proportional to the total reaction velocity $\Gamma = \Gamma^+ - \Gamma^-$ represent the reactive mass production of species s per $cm^3$ and per sec. The intercomponent convective terms in Equation (52) are the friction and thermodiffusion forces between the different components. In Equation (53), the term proportional to the total reaction velocity $\Gamma = \Gamma^+ - \Gamma^-$ is the reactive energy source in the s-component. The terms proportional to the temperature difference $\Delta T_{rs} = T_r - T_s$ represent the heat transfer between the components of unequal temperature. The following term represents the thermalization of the kinetic energy of the interpenetrating components due to the friction forces. The last term considers the power of the thermodiffusion forces.

## Transport Relations

The field equations are to be supplemented by the transport equations for the anisotropic part of the pressure tensor, $\vec{\vec{\pi}}_s = \vec{\vec{P}}_s - p_s \vec{\vec{U}}$, and heat current vector $\vec{q}_s$.

### Pressure Tensor

The general transport equation for the anisotropic part of the pressure tensor is obtained by applying the general equation of change, Equation (34), to the corresponding velocity moment. To make this transport equation convenient for applications, terms associated with heat currents and reaction influences and terms nonlinear in velocity gradients are neglected. Also, specializing for phenomena, which are slow compared to the relaxation time, $\tau_s$, for viscous momentum transfer, the final relation is:

$$\vec{\vec{\pi}}_s - 2 \ll \vec{\vec{\pi}}_s \times \vec{\omega}_s \gg \tau_s = - 2 p_s \tau_s \ll \nabla \vec{\vec{v}}_s \gg \tag{54}$$

Note that the cyclotron frequency vector, $\vec{\omega}_s = e_s \vec{B}/m_s$, depends on the sign of the respective charge, $e_s$. The relaxation times are for:[5,6,7]

Rigid Sphere Interactions:

$$\tau_s \equiv \tau_{ss} = \frac{5\sqrt{\pi}}{16} \sqrt{\frac{m_s}{k T_s}} \left( n_s Q_{ss} \right)^{-1} \tag{55}$$

$Q_{ss}$ from Equation (38);

Coulomb Interactions:

$$\tau_s \equiv \tau_{ss} = \frac{5\sqrt{\pi}}{16} \sqrt{\frac{m_s}{k T_s}} \left[ \frac{\ln \theta_{ss}}{\ln \theta_{ss} + \theta_{ss}^{-1} - 1} \right] \left( n_s Q_{ss} \right) - 1 \tag{56}$$

$Q_{ss}$ from Equation (40).

The vector product between a tensor and a vector is defined by

$$(\vec{\vec{T}} \times \vec{A})_{ij} = T_{ki} \epsilon_{jkl} A_l \tag{57}$$

where $\epsilon_{jkl}$ is the permutation tensor. For two vectors $\vec{A}$ and $\vec{B}$, the symmetric traceless tensor is defined as

$$<<\vec{A}\,\vec{B}>>_{ij} = \frac{1}{2}\left(A_i B_j + B_i A_j - \frac{2}{3}\delta_{ij} A_k B_k\right) \tag{58}$$

As an example, consider a plasma with the magnetic field in the y-direction. In this case, the solution of Equation (55) is:

$$\pi_{s,xx} = -\frac{2\mu_s}{1+4\omega_s^2\tau_s^2}\left[u_{s,xx} + \frac{1}{2}(u_{s,xx}+u_{s,zz})\,4\omega_s^2\tau_s^2 - u_{s,xz}\,2\omega_s\tau_s\right]$$

$$\pi_{s,yy} = -2\mu_s\, u_{s,yy}$$

$$\pi_{s,zz} = -\frac{2\mu_s}{1+4\omega_s^2\tau_s^2}\left[u_{s,zz} + \frac{1}{2}(u_{s,zz}+u_{s,xx})\,4\omega_s^2\tau_s^2 + u_{s,zx}\,2\omega_s\tau_s\right]$$

$$\pi_{s,xy} = \pi_{s,yx} = -\frac{2\mu_s}{1+\omega_s^2\tau_s^2}\left[u_{s,xy} - u_{s,yz}\,\omega_s\tau_s\right] \tag{59}$$

$$\pi_{s,xz} = \pi_{s,zx} = -\frac{2\mu_s}{1+4\omega_s^2\tau_s^2}\left[u_{s,xz} + \frac{1}{2}(u_{s,xx}-u_{s,zz})\,2\omega_s\tau_s\right]$$

$$\pi_{s,yz} = \pi_{s,zy} = -\frac{2\mu_s}{1+\omega_s^2\tau_s^2}\left[u_{s,yz} + u_{s,xy}\,\omega_s\tau_s\right]$$

The viscosity has been defined in the usual way,

$$\mu_s \equiv p_s\,\tau_s \tag{60}$$

The tensor components $u_{s,ij}$ are abbreviations for the components of the tensor $<<\nabla\vec{v}_s>>$.

Heat Current

The general transport equation for the heat current vector is obtained by applying the general equation of change, Equation (34), to the corresponding velocity moment. As in the previous case, various simplifications are introduced. Neglected are: (1) terms proportional to the gradients of the velocity fields; (2) terms connected with gradients of the nonisotropic pressure tensor; and (3) reaction influences. Restricting again to phenomena, which are slow compared to the characteristic relaxation time $\tau_s^* \equiv \frac{3}{2}\,\tau_s$, Equations (55-56), it follows for the regarded transport equation:

$$\vec{q}_s - \vec{q}_s \times \vec{\omega}_s \tau_s^* = -\frac{5}{2}\frac{k}{m_s} p_s \tau_s^* \nabla T_s + \tau_s^* \vec{\delta}_s \tag{61}$$

The analytical solution of this equation is explicitly:

$$\vec{q}_s = -\frac{1}{1+\omega_s^2 \tau_s^{*2}} \left\{ \left(\lambda_s \nabla T_s - \tau_s^* \vec{\delta}_s\right) + \left[\vec{\omega}_s \tau_s^* \cdot \left(\lambda_s \nabla T_s - \tau_s^* \vec{\delta}_s\right)\right] \vec{\omega}_s \tau_s^* - \vec{\omega}_s \tau_s^* \times \left(\lambda_s \nabla T_s - \tau_s^* \vec{\delta}_s\right) \right\} \tag{62}$$

where the thermal conductivity is defined as

$$\lambda_s \equiv \frac{5}{2}\frac{k}{m_s} p_s \tau_s^* \tag{63}$$

The forces which produce the thermal currents are temperature gradients, $\nabla T_s$, and diffusion forces, $\vec{\delta}_s$, of interpenetrating components with different particle masses (Dufour effect)[6]

$$\vec{\delta}_s = 8\sqrt{\frac{2}{\pi}} \sum_{r \neq s} n_s n_r Q_{sr} \frac{\left(\mu_{sr} k T_{sr}\right)^{3/2}}{m_s^2} \epsilon_{sr} \left(\vec{\bar{v}}_r - \vec{\bar{v}}_s\right) \tag{64}$$

According to the applying law of interaction, the coefficients are:[6]

Rigid Sphere Interactions:

$$\epsilon_{sr} = \left[\frac{8}{3} - 3\frac{T_s}{T_{sr}} + \frac{1}{2}\frac{T_s^2}{T_{sr}^2}\right]$$

Coulomb Interactions:

$$\epsilon_{sr} = \left[\left(\frac{T_s}{T_{sr}} - \frac{3}{2}\frac{T_s^2}{T_{sr}^2}\right) + \frac{4}{3 \ln \theta_{sr}}\left(1 - \frac{T_s}{T_{sr}}\right)\right]$$

The thermodiffusion effect, Equation (64), is of the intercomponent convective type and, therefore, of primary importance for the possible nonequilibrium which can establish between the components.

Further Remarks

In the presented description of reacting multitemperature plasma, excitation reactions are included only by means of a corrective factor. In principle, a more exact treatment of excitation reactions and, consequently, also of ionization reactions from excited levels, is possible as the reaction coefficients, Equations (46) and (47), can be applied to any level. However, the number of equations would be increased considerably, as alone for every particle kind in excited state n (n = 1, 2, 3, ...$\infty$) a separate conservation equation has to be formulated. For this reason, following Elwert,[9] a phenomenological factor, $\xi$, correcting for the excitation reactions has been introduced. In low temperature plasmas, $\xi \rightarrow 1$ can be assumed when the atoms are practically in the ground state.

Another point is the convergence of the series development of the velocity distribution function, Equation (36). Obviously, the anisotropic pressure components must be small compared to the static pressure,

$$\left|\pi_{s,ij}\right| << p_s,$$

and the heat current vector components must satisfy the condition,

$$\left|q_{s,i}\right| << \frac{1}{n_s m_s \left(\frac{k T_s}{m_s}\right)^{3/2}}$$

In continuously operated converter plasmas, these relations are, in general, satisfied, as the gradients of the velocity and temperature fields can be considered to be small. In a shock wave structure, with strong inhomogeneities of the fields, for comparison, the conditions may well be violated. The perturbation of the distribution functions by the reactions, finally, should be negligible in the considered temperature range.

Reference to this part of the report will be made in various applications which are in progress.

## VI. BIBLIOGRAPHY


1. Tolman, R. C. Principles of Statistical Mechanics. Oxford, 1938.

2. Muenster, A. Handbuch der Physik. III. 2. Berlin: Springer, 1959.

3. Schiff, L. I. Quantum Mechanics. McGraw-Hill, 1952.

4. Landau, L. D. Z. Physik. 64, 629 (1930).

5. Schrade, H. et al. Z. Naturforschg. 15a, 155 (1960).

6. Schindler, M. Diploma Thesis, Technical University, Stuttgart (1963).

7. Chapman, S. and Cowling, T. G. The Mathematical Theory of Nonuniform Gasses. Cambridge, 1952.

8. Grad, H. Comm. Pure Appl. Mathematics. 2, 331 (1949).

9. Elwert, G. Z. Naturforschg. 7a, 432 (1952).

## DISTRIBUTION LIST

| | No. copies |
|---|---|
| Director, Advanced Research Projects Agency<br>The Pentagon<br>Washington, D. C. 20301<br>Attn: Dr. John Huth | 2 |
| Office of Naval Research<br>Power Branch (Code 429)<br>Washington, D. C. 20360<br>Attn: John A. Satkowski | 6 |
| Commanding Officer<br>Office of Naval Research Branch Office<br>Box 39 Navy #100 Fleet Post Office<br>New York, New York | 1 |
| Cognizant ONR Area Branch Office | 1 |
| U. S. Naval Research Laboratory<br>Washington 25, D. C.<br>Attn: Technical Information Division | 6 |
| Wright-Patterson Air Force Base<br>Aeronautical Systems Division<br>Ohio<br>Attn: Don Warnock (ASRMFP-2) | 1 |
| Air Force Office of Scientific Research<br>Washington 25, D. C.<br>Attn: Dr. Milton M. Slawsky | 1 |
| U. S. Naval Ordnance Test Station<br>Propulsion Applied Research Group<br>China Lake, California<br>Attn: Leroy J. Krzycki (Code 4506) | 1 |
| Rome Air Development Center<br>Rome, New York<br>Attn: Mr. Frank J. Mellura | 1 |

| | No. copies |
|---|---|
| U. S. Naval Ordnance Laboratory<br>NA Division<br>White Oak, Maryland | |
| Attn: Wallace Knutsen | 1 |
| Library | 2 |
| Defense Documentation Center<br>Cameron Street<br>Alexandria, Virginia 22314 | 20 |
| U. S. Army Research & Development Laboratory<br>Fort Belvoir, Virginia | |
| Attn: Frank Shields (ERD-EP) | 1 |
| NASA, Lewis Research Center<br>21,000 Brookpark Road<br>Cleveland 35, Ohio | |
| Attn: Wolfgang Moeckel | 1 |
| Dr. B. Lubarsky | 1 |
| U. S. Atomic Energy Commission<br>Division of Reactor Development<br>Direct Energy Conversion Section, RD; AED<br>Germantown, Maryland | 1 |
| Dr. T. Brogan<br>AVCO - Everett Research Laboratory<br>2385 Revere Beach Parkway<br>Everett, Massachusetts | 1 |
| Dr. J. Cole<br>Department of Aeronautics<br>California Institute of Technology<br>Pasadena, California | 1 |
| Mr. Arthur Sherman<br>General Electric - Valley Forge<br>Valley Forge Space Technical Center<br>Philadelphia 1, Pennsylvania | 1 |

| | No. copies |
|---|---|
| Dr. M. Talaat<br>Martin Marietta Corporation<br>Nuclear Division<br>Baltimore 3, Maryland | 1 |
| Dr. W. D. Jackson<br>Electrical Engineering Department<br>Massachusetts Institute of Technology<br>Cambridge 39, Massachusetts | 1 |
| Dr. Vernon H. Blackman<br>MHD Research Incorporated<br>1535 Monrovia Street<br>Newport Beach, California | 1 |
| Dr. B. C. Lindley<br>Nuclear Research Centre<br>C. A. Parsons & Co., Ltd.<br>Fossway, Newcastle Upon Tyne 6<br>England | 1 |
| Dr. Robert Eustis<br>Thermosciences Division<br>Stanford University<br>Standford, California | 1 |
| Mr. John Wright<br>Central Electricity Research Laboratories<br>Cleeve Road, Leatherhead, Surrey<br>England | 1 |
| Dr. Richard Schamberg<br>Rand Corporation<br>1700 S. Main Street<br>Santa Monica, California | 1 |
| Dr. Sam Naiditch<br>Unified Science Associates<br>826 Arroyo Parkway<br>Pasadena, California | 1 |

| | No. copies |
|---|---|
| Dr. W. S. Emmerich<br>Westinghouse Research Laboratories<br>Beulah Road, Churchill Borough<br>Pittsburgh 35, Pennsylvania | 1 |
| Dr. R. T. Schneider<br>Allison Division<br>General Motors Corporation<br>Indianapolis, Indiana | 1 |
| Dr. D. G. Elliott<br>Jet Propulsion Laboratory<br>Pasadena, California | 1 |

UNCLASSIFIED